Anticyclonic eddies aggregate pelagic predators in a subtropical gyre

Arostegui MC [1,2*] Gaube P[1] Woodworth-Jefcoats PA[3] Kobayashi DR[3] Braun CD[2,4]

1. Air-Sea Interaction and Remote Sensing Department, Applied Physics Laboratory, University of Washington, Seattle, WA, USA
2. Biology Department, Woods Hole Oceanographic Institution, Woods Hole, MA, USA
3. Ecosystem Sciences Division, Pacific Islands Fisheries Science Center, National Marine Fisheries Service, National Oceanic and Atmospheric Administration, Honolulu, HI, USA
4. School of Aquatic and Fishery Sciences, University of Washington, Seattle, WA, USA

* Correspondence author. Email: martin.arostegui@whoi.edu

Key words: mesoscale, eddy, subtropical gyre, deep scattering layer, micronekton, diel vertical migration

Ocean eddies are coherent, rotating features that can modulate pelagic ecosystems across multiple trophic levels. These mesoscale features, which are ubiquitous at mid-latitudes [1], may increase productivity of nutrient-poor regions [2, 3], accumulate prey [4], and modulate habitat conditions in the water column [5]. However, in nutrient-poor subtropical gyres - the largest marine biome - the role of eddies in modulating behavior throughout the pelagic predator community remains unknown despite predictions for these gyres to expand [6] and pelagic predators to become increasingly important for food security [7]. Using a large-scale fishery dataset in the North Pacific Subtropical Gyre, we show a pervasive pattern of increased pelagic predator catch inside anticyclonic eddies relative to cyclones and non-eddy areas. Our results suggest that increased mesopelagic prey abundance in anticyclone cores [4, 8] may be attracting diverse predators, forming ecological hotspots where these predators aggregate and exhibit increased abundance. In this energetically quiescent gyre, we expect that isolated mesoscale features (and the habitat conditions within them) exhibit primacy over peripheral submesoscale dynamics in structuring the foraging opportunities of pelagic predators. Our finding that eddies influence coupling of epi- to mesopelagic communities corroborates the growing evidence that deep scattering layer organisms are vital prey for a suite of commercially-important predator species [9] and, thus, provide valuable ecosystem services.

Main

Mesoscale eddies are rotating bodies of water that have spatial scales of order 10–100 km, can persist for weeks to years, and have been estimated to cover in excess of 30% of ocean surface area in the mid-latitudes [1]. These coherent features generate lateral and vertical gradients in the physical structure of the ocean by trapping and transporting large water masses across vast distances [5] and by driving the vertical flux of heat and nutrients which, in turn, can modulate primary production [10].

A growing body of evidence suggests that mesoscale eddies modulate pelagic ecosystems beyond their effect on photoautotrophs, with impacts reaching the highest trophic levels. Surveys in the North Atlantic have revealed that eddies may affect the biomass of mesopelagic ecosystems [8, 11], the fauna of which likely constitute a crucial prey resource for large pelagic predators [9, 12]. Multiple mechanisms by which mesoscale eddies influence the behavior of large pelagic predators have been suggested, including the accumulation of micronekton (thereby forming oceanic hotspots for predators [4]) and modulation of the thermal structure of the water column (potentially regulating predator access to mesopelagic resources [13, 14]). Documentation of pelagic predators remaining within mesoscale eddies for months at a time highlights their potential role as rich foraging grounds in the open ocean[15].

Subtropical gyres constitute the largest marine biome at $> 40\%$ of the world ocean's surface [6], but support exceptionally low predator densities under conditions of nutrient scarcity in surface waters [16]. Mesoscale eddies may increase productivity in these otherwise nutrient-poor regions [2, 3]. However, it remains unknown if this physical-biological interaction modulates pelagic predator behavior in a conserved manner across diverse taxa and if behavioral responses to eddies in subtropical gyres are consistent with those of more productive regions. While there is a rapidly growing body of research showing widespread affiliation to mesoscale eddies across diverse predator taxa, there have been no community-level assessments of pelagic predator association with eddies within a subtropical gyre. This knowledge gap is underscored by predictions for this biome to expand in area in response to global warming [6].

Here, we integrate satellite observations of mesoscale eddies with pelagic predator catch data from the Hawaiian deep-set longline fishery – one of the largest and highest revenue fisheries in the North Pacific Subtropical Gyre [17] – to investigate how mesoscale eddies modulate pelagic ecosystems in a nutrient-poor environment. This gyre supports a number of predator species that are central to the economic and food security of Pacific Islands nations and communities, and that are predicted to become increasingly important in maintaining healthy nutrition of their people [7]. However, pelagic predators in the North Pacific Subtropical Gyre have exhibited significant long-term decreases in relative abundance [18]. This mismatch highlights

the necessity of understanding the potential biophysical drivers of predator behavior so as to better inform effective management of these species, their supporting ecosystems, and dependent fisheries. In leveraging an unprecedented quantity of community-level biological data co-occurring with eddies, this study proposes a paradigm fundamentally relating ocean energetics to ecologically relevant scales of physical-biological interaction that modulate foraging opportunity at the highest trophic levels.

Anticyclones Increase Catch of Predators

We co-located over 220,000 longline sets – yielding ∼6.5 million individual pelagic predators – to > 4,700 unique mesoscale eddies represented by > 91,000 daily eddy realizations (i.e., observations of an eddy on a given day). We focused on 14 of the most commonly captured pelagic predators, including those of commercial importance (such as bigeye tuna, the primary target of the fishery) as well as non-target bycatch (Table S1). Given the variability in size of mesoscale eddies, we established a common spatial frame of reference by delineating the different zones of these features in terms of distance from eddy center normalized by the eddy radius (R); the eddy core is the area enclosed by R, and the periphery is the area from the edge of the core to a distance of two eddy radii (R – $2R$).

Visualization of the nominal, co-located fishery data suggested eddy-centric patterns in predator catch (Figs. 1, S1-13). However, co-located fishing effort by the Hawaiian deep-set longline fleet spans > 13 million km^2 across the North Pacific Subtropical Gyre, within which there are two subregions of distinct eddy dynamics (Fig. S14). The division of these subregions is evident in the energy contained in the mesoscale eddy field, or eddy kinetic energy (EKE); there is (1) an area of relatively high EKE where winds are thought to drive eddy genesis in the lee of the Hawaiian Islands and nearby seamounts [19, 20] and (2) an area of relatively low EKE where such topographical features are not present [21] (Fig. S14). Thus, to more rigorously quantify eddy-driven effects on catch, we developed species-specific models assessing if eddy-related effects were present and either homogeneous across the North Pacific Subtropical Gyre or different among the subregions with distinct eddy dynamics. Furthermore, to minimize the effects of potentially confounding factors in our fishery-dependent dataset, we used this modelling approach to standardize catch probability and positive catch rate of each predator by explicitly accounting for higher-order environmental processes (e.g., large-scale spatial differences in distribution), variability in fishing methodology (e.g., gear configurations), and fisher behavior.

Catch standardization models accounting for mesoscale eddies exhibited the best fit to the fishery data for all 14 pelagic predators tested (Table S2). To interrogate the eddy-centric catch patterns, we used

model-estimated ratios comparing the species-specific mean catch odds and catch rate in each zone (e.g., inner core) of anticyclones against the same zone in cyclones. The *catch odds ratio* is the ratio of the odds of catching a particular species in a given zone of an anticyclone to the odds in the corresponding zone of a cyclone, and is thus derived from whether a longline caught the focal species (presence/absence). The *catch rate ratio* is the ratio of the non-zero incidence rate of a particular species in a given zone of an anticyclone to the non-zero incidence rate in the corresponding zone of a cyclone, and is thus derived from how many individuals of the focal species were caught on a longline yielding at least one individual (positive count).

Statistically significant catch odds and rate ratios occurred more often - and were typically of greater magnitude - among the eddy cores than among the peripheries (Figs. 2, S15). This resulted in a general trend for the difference in catch metrics between anticyclones and cyclones to be greatest in their cores where eddies are likely to exhibit the most anomalous biophysical environment relative to outside the area of eddy impact (Table S3, Fig. 1). Furthermore, most species exhibited significantly increased catch metrics in anticyclone cores relative to cyclone cores (Figs. 2, S15); mean catch odds and catch rates were as much as 79 and 83% higher, respectively, depending on the species and underlying eddy dynamics subregion. Eleven of fourteen species exhibited significantly higher catch metrics in anticyclone cores in the subregion characterized by high EKE, and twelve of fourteen species exhibited a similar trend in the low EKE subregion (Fig. S16). These consisted of the four tunas (albacore, bigeye, yellowfin, skipjack), four billfishes (striped marlin, blue marlin, shortbill spearfish, swordfish), wahoo, pomfret, and escolar in both regions and dolphinfish in only the low EKE subregion. In contrast, catch metrics were higher in cyclone cores for only three of fourteen species in the high EKE subregion (opah, blue shark, dolphinfish), and only one species in the low EKE subregion (opah). Averaging across species-specific estimates, the mean catch metrics were 8-21% higher in the core of anticyclones than cyclones (Table S3). Similarly, when summing the model-predicted mean catch responses for each of the 14 predator species (taking into account each species' relative contribution to the catch composition), the overall catch of the average longline set was 7-12% higher in the core of anticyclones than cyclones (Tables S4, S5).

To further contextualize these findings, we conducted a complementary catch standardization analysis comparing amongst the cores of eddies and areas devoid of eddy influence (i.e., beyond eddy peripheries). This comparison against a non-eddy baseline corroborated our eddy-centric results for this pelagic predator community, as catch metrics inside anticyclones were significantly greater than those in non-eddy areas for 7-10 species and significantly lower than those in non-eddy areas for only 0-2 species (Fig. S17). In contrast, catch metrics inside cyclones were significantly greater than those in non-eddy areas for only 1-2 species and significantly lower than those in non-eddy areas for 6-9 species (Fig. S17). Thus, there

was a general trend across the pelagic predator community for catch metrics to be highest in anticyclones, intermediate in non-eddy areas, and lowest in cyclones, regardless of the underlying eddy dynamics subregion (see Supplemental Results).

Mechanistic Drivers of Catch in Eddies

Mesoscale eddy effects on catch were ubiquitous and largely shared among this diverse assemblage of pelagic predators, suggesting that modulation of pelagic ecosystems by these features extends to the highest trophic levels. There are several potential mechanisms that may lead to the observed, pervasive pattern of increased pelagic predator catch inside anticyclone cores (Fig. 2). The fishery-dependent nature of the catch dataset analyzed here is influenced by three primary factors that affect differential catch of pelagic predators: abundance (the number of individuals of a given species present), susceptibility to being caught ("catchability"; the efficiency of fishing gear in sampling a species' abundance) and fishing effort (how much fishing gear is deployed and how many times) [22]. In our analysis, we explicitly account for effort, thereby isolating abundance and catchability as the most likely primary drivers of the disparity in catch metrics among eddy polarities and non-eddy areas.

Abundance

Mesoscale variability in abundance of pelagic predators is most likely to be influenced by selection for habitats hosting enhanced foraging opportunity (Fig. 3a). Telemetry studies have documented an affinity for the cores of anticyclones across a diverse range of predator taxa [13, 14, 23, 24, 25]. These eddy-centric affinities observed in free-ranging animals, as well as the catch patterns we documented, are consistent with recent studies that identified eddy-centric patterns in primary productivity [3, 26, 27] and the potential availability of mesopelagic prey [4, 8, 11]. Unlike in other biomes of the world ocean, anticyclones in all five subtropical gyres exhibit greater chlorophyll concentration [3, 26], phytoplankton with larger cell size [27], and, by extension, enhanced primary productivity at the ocean surface relative to cyclones. While the concomitant impacts of this productivity difference on the prey base at intermediate trophic levels are unknown, trophic transfer efficiency from phytoplankton up to micronekton in the deep scattering layer may be higher in nutrient-poor regimes relative to more productive waters [28]. Surveys in the North Atlantic have found that acoustic backscattering by deep scattering layer organisms was greater in the cores of anticyclones than their peripheries, cyclone cores, or areas beyond eddy influence [4, 8]; however, these studies all occurred poleward of the subtropical gyre where cyclones typically exhibit greater chlorophyll concentrations than anticyclones at the ocean surface. This apparent contradiction of greater micronekton backscattering occurring where

surface waters are characterized by low productivity suggests that subsurface features of anticyclones, such as enhanced depth-integrated productivity [29, 30, 31], may help to increase the potential availability of deep scattering layer prey in various biomes – but the mechanisms remain uncertain.

The greater acoustic backscatter found in the cores of anticyclones is evident both at mesopelagic depths during the day and epipelagic depths during the night [8]. This diel shift in prey depth distribution is a result of diel vertical migration, by which deep scattering layer organisms track ambient light levels [32, 33]. Approximately 90% of micronekton that comprise deep scattering layers exhibit diel vertical migration on a daily basis in the eastern Pacific [32], which results in greater nighttime than daytime biomass in the surface waters of the North Pacific Subtropical Gyre [33]. Pelagic predators in our study include species that have evolved physiological and sensory adaptations for accessing mesopelagic habitats (presumably to forage) as well as others that are largely limited to foraging in the epipelagic [9, 34]; yet, both behavioral guilds of predators potentially benefit from enhanced deep scattering layer biomass in anticyclone cores. Deep-foraging predators can benefit from enhanced deep scattering layer resources at the deepest point of the diel vertical migration cycle during the day (e.g., bigeye tuna [34]) and shallow-foraging predators can target many of these same prey species at the shallowest point of the diel vertical migration cycle at night (e.g., shortbill spearfish [35]). This aligns with studies that identified trophic linkages between mesopelagic micronekton and both behavioral guilds of pelagic predators [12, 36, 37]. Thus, the potentially increased biomass of deep-scattering layer organisms in anticyclone cores may attract a diverse assemblage of pelagic predators to form ecological hotspots in an otherwise nutrient-poor biome, leading to increased predator abundance and catch in these features. In contrast, cyclones have recently been associated with lower integrated mesopelagic backscattering [8, 11] and further study is needed to understand why a small subset of ecologically diverse predator taxa might associate with these features.

Catchability

Depending on polarity, eddy-driven changes to vertical structure of the water column often result in positive (warm) or negative (cold) temperature anomalies at depth. These changes may serve to expand or contract the vertical habitat available to pelagic predators, which governs the degree of overlap between fishing gear and predator habitat use and, thereby, modulates catchability (Fig. 3b, [38]). Endothermic white sharks and ectothermic blue sharks in the Gulf Stream region of the NW Atlantic dive farther into the mesopelagic and spend more time at those depths while in the anomalously warm cores of large amplitude anticyclones compared to the colder cores of cyclones, suggesting that the downward displacement of isotherms at depth in anticyclones alleviates thermal constraints to deep-diving and presumably facilitates access to deep scattering

layer organisms [13, 14]. In contrast, white and blue sharks do not exhibit significantly different depth distributions among eddies characterized by comparatively smaller differences in vertical thermal structure, such as those of low amplitude originated from the North Atlantic Subtropical Gyre [13, 14]. Together, these results suggest that high amplitude anticyclones that drive anomalously warm conditions at depth (e.g., +4°C, ∼200 m deepening of isotherms compared to cyclones) can enable otherwise thermally-limited predators to expand their use of the water column and spend significantly more time at depth. In eddies, the relationship between polarity and catchability is theoretically determined by whether the typical depth distribution of the predator species is shallower or deeper than that of the fishing gear and if the direction of isotherm displacement increases their overlap.

Despite these potential impacts of eddies on vertical habitat use of pelagic predators, composites of eddies within the North Pacific Subtropical Gyre suggest that eddy-driven changes to the vertical temperature structure (Fig. S18) consist of, on average, $< +2$°C, 100 m isotherm displacement in anticyclones relative to cyclones (and even less relative to the areas outside of eddies). These differences are smaller than those of low amplitude eddies within the North Atlantic Subtropical Gyre [13] and, thus, likely have negligible impacts on vertical habitat use of pelagic predators. This suggests that potential changes in catchability caused by eddy-driven vertical habitat expansion or compression are likely minimal in the North Pacific Subtropical Gyre and that this mechanism is unlikely to be an important driver of the observed catch patterns.

Mesoscale Dominance in the Gyre

Contrasting our results with those of other studies highlights uncertainties in whether physical-biological interaction at the mesoscale versus submesoscale primarily drives pelagic predator behavior. For example, a number of other studies have suggested that predators associate more closely with the edges of eddies than their cores [39]. Such results may, in part, be explained by the accumulation of plankton biomass at submesoscale (order 1–10 km) fronts generated between interacting mesoscale features [40], a phenomenon that is not replicated by isolated eddies [41]. These fronts create a nutrient exchange route between the ocean surface and depths, potentially providing predators with enhanced foraging opportunities along the edges of interacting eddies [42].

Our study indicates a pervasive pattern of increased catch in anticyclone cores in the North Pacific Subtropical Gyre, whereas past studies identifying predator affinity for mesoscale eddies or submesoscale fronts were largely conducted in more energetic oceanographic regimes. The North Pacific Subtropical Gyre is characterized by low amplitude eddies that generate less strain, which should yield fewer derived submesoscale fronts

[43] – especially if interactions among mesoscale features in this biome are weaker and less likely to occur. Generation of submesoscale features along the periphery of eddies during eddy-eddy interaction has been observed in the North Pacific Subtropical Gyre [44], but this phenomenon only becomes widespread under anomalous conditions [45]. Among the five subtropical gyres, the ratio of mesoscale versus submesoscale contributions to large, positive increases in surface chlorophyll is highest in the North Pacific [46]. The magnitude and abundance of submesoscale instability in this region is limited by the shallow, relatively stable surface mixed layer that constrains the energy available for such motions [43]. Thus, we propose a new paradigm in which isolated mesoscale features in quiescent regions, such as subtropical gyres, exhibit primacy over peripheral submesoscale dynamics in structuring the foraging opportunities of pelagic predators; however, in more energetic biomes, we expect the bidirectional energy fluxes among the mesoscale and submesoscale [47] to markedly increase the relevance of submesoscale features.

Discussion

Our findings suggest that anticyclonic mesoscale eddies serve to aggregate a diverse pelagic predator community in the North Pacific Subtropical Gyre, likely as a result of enhanced deep scattering layer biomass in their cores. This corroborates the potential significance of connectivity among the epipelagic and mesopelagic zones, which must be considered in impact assessments of future deep-sea industries. Burgeoning interest in deep scattering layer fisheries is confronted by the limited information on deep-sea ecology and the potential ecosystem impacts of micronekton extraction [48]. It is unclear how much deep scattering layer biomass can be removed by fisheries without exerting a detrimental impact on dependent predators or the ocean's capacity for carbon sequestration and climate regulation [49]. Improving our understanding of the ecosystem services provided by mesopelagic communities, particularly with respect to their role as forage for pelagic predators and thereby in supporting predator fisheries central to global food security [49], is necessary to inform responsible use of deep ocean resources. The modulation of pelagic ecosystems across multiple trophic levels by mesoscale eddies highlights the complex physical-biological interactions that drive coupling of epi- to mesopelagic communities and influence the sustainability of forage and predator fisheries in the world ocean.

Data Availability

Fisheries data used in this paper are subject to confidentiality of information requirements under the Magnuson–Stevens Fishery Conservation and Management Act and are not available to the public except in summary aggregate form. Information on requesting access to these data can be found at https://

inport.nmfs.noaa.gov/inport/item/2721 (logbook data) and https://www.fisheries.noaa.gov/inport/item/9027 (observer data). The oceanographic data used in this study are publicly available from AVISO's Mesoscale Eddy Trajectory Atlas (https://www.aviso.altimetry.fr/en/data/products/value-added-products/global-mesoscale-eddy-trajectory-product.html), the EU Copernicus Marine Environment Monitoring Service (CMEMS, https://marine.copernicus.eu/), and NOAA National Center for Environmental Information's Argo Data Repository (https://www.nodc.noaa.gov/argo/floats_data.htm). All information graphed or tabulated in this paper is nonconfidential.

Code Availability

Eddy co-location code and catch-effort standardization code are provided with this manuscript.

Funding

MCA, CDB, and PG were supported by the NASA New Investigator Program 80NSSSC20K1132, MCA and PG were also supported by NOAA project NA15OAR4320063, MCA was also supported by the Postdoctoral Scholar Program at Woods Hole Oceanographic Institution with funding provided by the Dr. George D. Grice Postdoctoral Scholarship Fund, and CDB was also supported by the NASA Earth Science Research Program 80NSSC19K0187 and The Investment in Science Program with funds from Woods Hole Oceanographic Institution.

Acknowledgements

We thank Les Gallagher (Fishpics® Illustrations) for producing artwork used in figures 1, 3, and 4, and Kim Reading and Maia LeDoux (UW APL) for producing figure 4. Jon Brodziak (NOAA PIFSC) and Ryan Rykaczewski (NOAA PIFSC) reviewed a version of this manuscript prior to submission.

Author Contributions

MCA contributed to study design, conducted analyses, wrote the manuscript, and helped acquire funding; PG contributed to study design, analyses, interpretation, revision, and funding acquisition; PAWJ contributed to study design and revision; DRK contributed to study design, revision, and funding acquisition; CDB contributed to study design, analyses, interpretation, revision, and funding acquisition.

Competing Interests

The authors declare no competing interests.

1 Figures

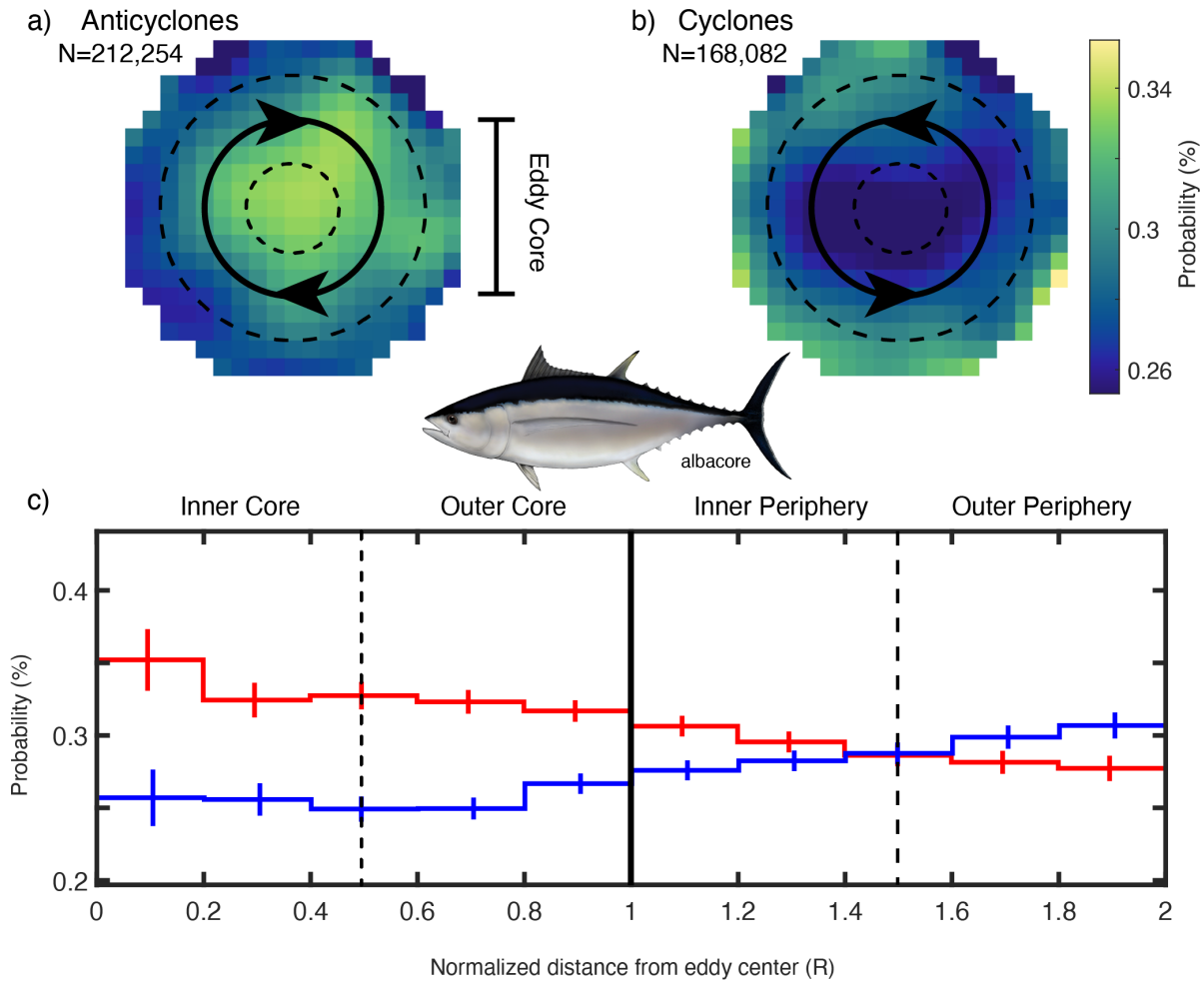

Figure 1: Nominal eddy-centric albacore catch: Example eddy-centric 2D (a, b) and 1D (c) composites of albacore catch probability – the % of longline sets catching at least one albacore – from the nominal fishery data across the study region. In panels a–c, the eddy core ($0 - R$) and periphery ($R - 2R$) are separated by the solid black line, and the inner and outer zones of both the core ($0 - 0.5R$ & $0.5R - R$) and periphery ($R - 1.5R$ & $1.5R - 2R$) are separated by the dashed black lines. In panels a and b, N represents the total number of individuals captured in eddies of the respective polarities, catch probability is calculated per $0.2R$ x $0.2R$ cell, and north is up. In panel c, N per polarity is the same as in panels a and b, anticyclonic values are red and cyclonic values are blue, and polarity-specific mean catch probability (with the 95% confidence interval) is calculated per $0.2R$ width bin. Number of longline sets in the catch composites (anticyclones: 113,966 | cyclones: 106,068).

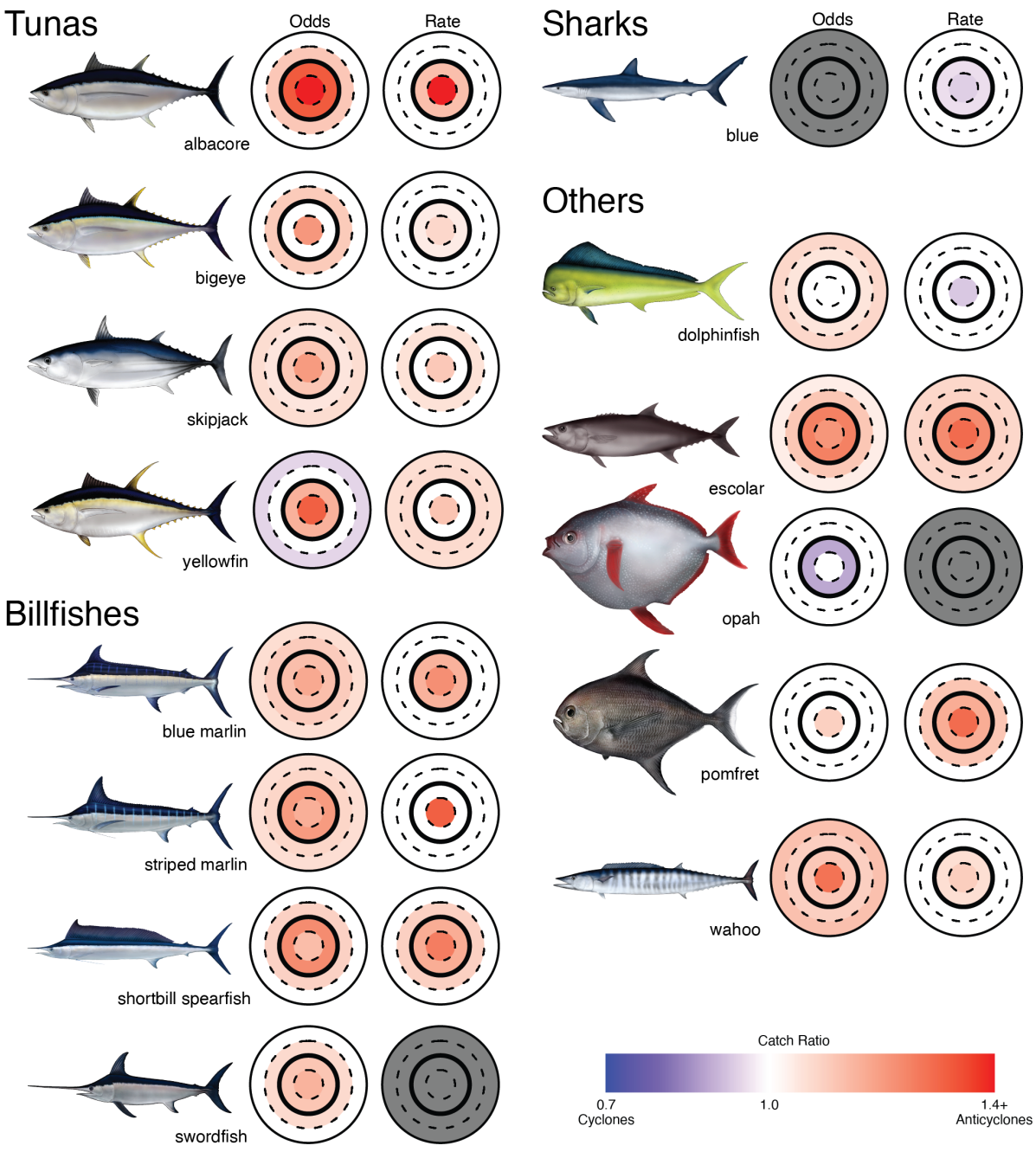

Figure 2: Eddy-centric catch metrics (high EKE): Catch odds ratios and catch rate ratios comparing a given zone of anticyclones against the corresponding zone of cyclones. Ratios of catch metrics are color coded; > 1 - significantly higher in anticyclones (red), < 1 - significantly higher in cyclones (blue), $= 1$ - not significantly different among polarities (white), N/A - best-fit model did not include eddy-related effects for that metric (grey). Ratio values > 1.4 were truncated to aid in color discernment. Ratios not significantly different among polarities were set to equal 1. Eddy cores are separated from peripheries by the solid black line, and both are further differentiated into inner and outer zones by the dashed black lines. These model-estimated ratios come from the high EKE subregion, but see Fig. S15 for the ratios from the low EKE subregion and Fig. S16 for the full results (ratios in both the high and low EKE subregions, including 95% confidence intervals determined with the delta method).

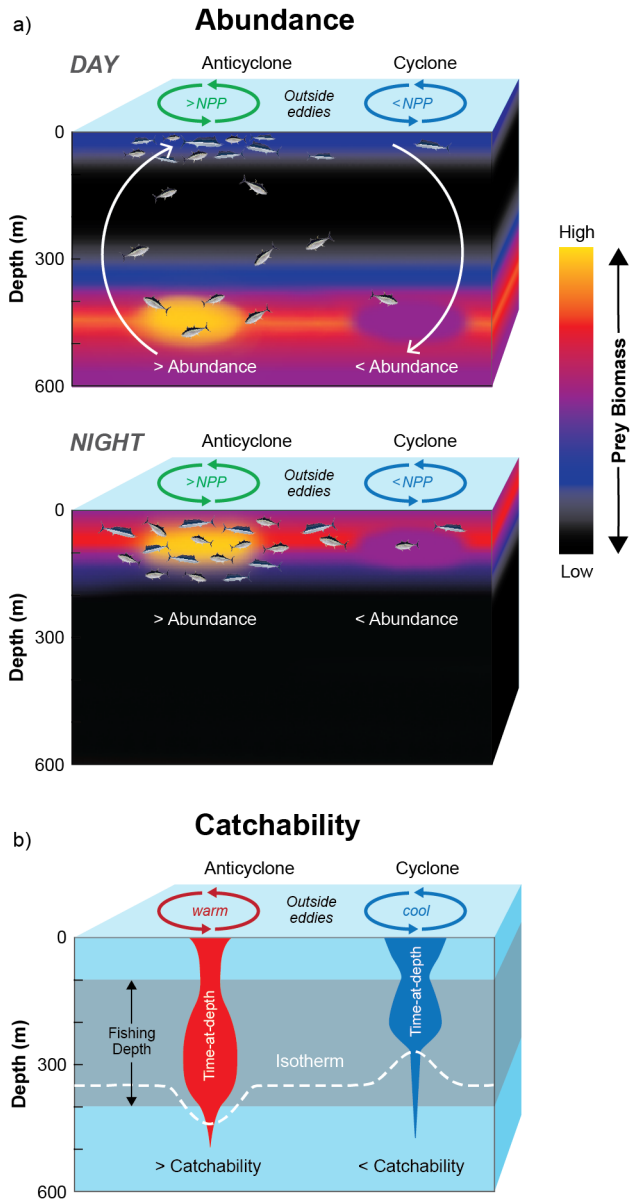

Figure 3: Potential mechanisms driving catch: Conceptualization of how differences in pelagic predator abundance (a) and catchability (b) may mechanistically drive a disparity in catch metrics among eddy polarities (and areas outside eddies). In regards to abundance (a), enhanced net primary productivity (NPP) in anticyclones of subtropical gyres may support increased deep scattering layer biomass, attracting predators and increasing their abundance within the cores of these features. During the daytime, only deep-foraging predators (such as bigeye tuna that repeatedly dive [white arrows]) may access the deep scattering layer at depth whereas shallow-foraging predators (such as shortbill spearfish) are restricted to surface waters. During the nighttime, when prey undergo diel vertical migration into surface waters, both deep- and shallow-foraging predators may access the deep scattering layer. In regards to catchability (b), the downward displacement of isotherms inside anticyclones may expand or shift a predator's depth distribution deeper, whereas the upward displacement inside cyclones may contract or shift that distribution shallower. Increased catchability in anticyclones is shown in this example but the relationship between eddy polarity and catchability is theoretically determined by the typical depth distribution of the predator species relative to that of the fishing gear and the direction of isotherm displacement.

References

paste first 49 references here from the master reference list generated at the end of the compiled PDF

Online content: Anticyclonic eddies aggregate pelagic predators in a subtropical gyre

2 Methods

2.1 Fishery Logbook Data

The deep-set sector of the Hawaiian longline fishery is legally identified by the number of hooks used between floats on the longline (≥ 15) and primarily fishes at 100 – 400 m depth during the daytime in (sub)tropical waters from 5 – 35°N to target tunas [50, 51, 52]. While these fishing operations are intended to catch species exhibiting a deeper daytime distribution, species exhibiting a shallower daytime distribution may be captured during gear deployment or retrieval as the gear passes through surface waters as well as on the shallowest hooks while the gear is settled at the target fishing depth [53]. Catches from the fishery are recorded by the fishers operating the vessels (hereafter referred to as the 'logbook' data). Using 23 yr of logbook data from 1995 – 2017, we restricted our analysis to 14 of the most commonly captured species of target and non-target pelagic predators in the fishery. Most of these pelagic predators are recorded in the logbooks as individual species categories (albacore - *Thunnus alalunga*; bigeye tuna - *Thunnus obesus*; yellowfin tuna - *Thunnus albacares*; skipjack tuna - *Katsuwonus pelamis*; striped marlin - *Kajikia audax*; blue marlin - *Makaira nigricans*; shortbill spearfish - *Tetrapturus angustirostris*; swordfish - *Xiphias gladius*; wahoo - *Acanthocybium solandri*), but the remainder are recorded in grouped species categories in which, typically, one species is predominant (blue shark - largely *Prionace glauca*; dolphinfish - largely *Coryphaena hippurus*; pomfret - largely *Taractichthys steindachneri*; escolar - largely *Lepidocybium flavobrunneum*; opah - *Lampris incognitus* and *L. megalopsis*).

Comparison of logbook data versus those recorded by federal fishery observers (hereafter referred to as the 'observer' data) highlights a source of uncertainty in our analysis. The logbook data are far more extensive (only 20% of deep-set fishing effort is observed annually) but the self-reporting they rely upon influences their accuracy. Species misidentifications and non-reporting events (e.g., counting landings rather than captures) are present, and less of the variables describing operational characteristics of the fishing gear (e.g., set timing and duration) are available in the logbook than observer data [54]. Yet, a previous study comparing logbook and observer annual catch-per-unit-effort trends for 10 of the 14 predator species used in this analysis found

correlations (r) ≥ 0.76, revealing them to be largely similar [18].

2.2 Co-location with Eddies

Individual longline sets at the location of their retrieval were co-located to eddies identified in the Mesoscale Eddy Trajectory Atlas available from AVISO (https://www.aviso.altimetry.fr/en/data/products/value-added-products/global-mesoscale-eddy-trajectory-product.html). This product tracks eddies that reach an age ≥ 28 days on a daily basis and includes both the latitude/longitude center and speed-based radius (R) of each feature throughout its lifetime [5]. We defined R as the radius of a circle with area equal to that enclosed by the streamline of the maximum average geostrophic speed of the eddy (equivalent to L_s in [5]). This radial distance is used to define the zones of an eddy relative to its center following [24], where a normalized distance of 0 is the center, distances < 1 indicate the core (i.e., interior) of the eddy, > 1 but < 2 indicate the periphery of the eddy, and > 2 indicate waters outside of the physical impact of the eddy. The calculation of a given longline set's normalized distance from eddy center consisted of dividing the Great Circle distance between the location of longline retrieval and the nearest eddy center by R of that eddy. We excluded longline sets that occurred within the Kuroshio Extension or north of 40°N (where almost no fishing effort occurred during the study period) as well as south of 10°N (where mesoscale variability is dominated by equatorial processes, such as tropical instability waves, and not by coherent mesoscale eddies). These filtering steps, as well as the removal of longline sets with missing data for terms included in model-standardization (see section 2.4), yielded a filtered logbook dataset of 318,200 longline sets of which 27, 42, and 31% occurred in eddy cores, eddy peripheries, and waters outside the physical impact of eddies, respectively.

Our collocation of longline sets to eddies using the location of retrieval (Fig. S19) entails some uncertainty in the assigned eddy zone. Longlines are deployed at one location and later retrieved at another, and the exact spatial coverage of the longline during that time (approximately dawn to dusk) is unknown given the use of a single spatial coordinate pair to co-locate fishing gear that was, on average, 56 km in length to eddies that were, on average, 109 km in radius (equivalent to 54.5 km per eddy zone). Thus, not all the catch of a given longline set occurs at the location of retrieval, meaning that a set assigned to a particular eddy zone may actually have (for example) captured some fish from an adjacent zone. Because the logbook data contain only the position of the vessel and not the extent of trailing gear (precluding use of an alternative metric such as the mid-point between the start and end locations of both termini of the longline), we use the location of retrieval start as representative of the gear over the course of its deployment. Thus, we cannot rule out the potential for a given longline set to result in catches across eddy zones. However, given the increasingly larger areas covered by eddy zones farther from the core (i.e., the eddy periphery encompasses a larger area than

the eddy core), our assignment of eddy zone results in longline sets with across-zone mixed catches being more frequently assigned to the larger area (e.g., the outer versus inner core) by chance. The relatively small size of eddy cores should thus result in the most significant reduction of longline sets being collocated to eddy cores compared to the periphery, thus diluting the actual catch in eddy cores relative to adjacent eddy areas. Yet, our findings indicate significantly elevated catch in eddy cores for most species, suggesting our results are likely conservative and robust to this source of potential uncertainty.

2.3 Delineating regions using eddy kinetic energy

The greater region covered by the Hawaiian deep-set longline fishery was divided into two subregions characterized by relatively high and low eddy kinetic energy (EKE). EKE was computed using high-pass filtered sea level anomaly (SLA) fields obtained from the EU Copernicus Marine Environment Monitoring Service (CMEMS, https://marine.copernicus.eu/) global reprocessed product. The SLA fields were high-pass filtered with a half-power cutoff of 20° in longitude and 10° in latitude resulting in a sea surface height (SSH) field free of the effects of seasonal heating and cooling [5]. Geostrophic currents were computed from the SSH fields and EKE was computed as:

$$EKE = \frac{\left(u^2 + v^2\right)}{2}.$$

where u and v are the zonal and meridional geostrophic currents, respectively. The climatological average EKE field was subsequently smoothed with a loess smoother with $7° \times 7°$ span enabling us to define the two subregions by the 150 $cm^2 s^{-2}$ contour (Fig. S14). This span and contour were chosen to yield geographically contiguous subregions.

2.4 Model-Standardization of Logbook Data: Eddy-Centric Analysis

To conduct an eddy-centric analysis of the logbook data focusing on potential differences among anticyclones and cyclones, we excluded longline sets that occurred > 2 normalized distances from the nearest eddy center (i.e., in areas devoid of eddy influence). From the filtered logbook dataset of 318,200 longline sets, we analyzed 220,034 longline sets that occurred in the core or periphery of 4,726 unique eddies (representing 91,185 daily eddy realizations) and caught a combined total of 6,408,818 fish across the 14 aforementioned pelagic predator taxa. Note that the blue shark model utilized 197 longline sets less than all other species due to non-reporting of those particular catches.

To identify and quantify the potential for eddies to modulate the catch of pelagic fishes, we built models with

and without eddy-related terms of varying complexity that also standardized for variability in catch arising from higher-order environmental processes and different fishing methodologies. Catch-effort standardization is needed to use fishery-dependent data as an index of abundance, as it removes the effects of factors other than abundance that may influence the observed catch [22]. To achieve this standardization, we used hurdle generalized linear mixed models (GLMMs) that modeled catch (in numbers of fish) as the response. A hurdle model is comprised of two components; (1) a presence/absence component determining whether a hurdle is overcome (i.e., whether a longline catches a particular species), and 2) a positive count component determining how many of something there are if the hurdle is overcome (i.e., when a species is present in a given longline set, how many individuals of that species are caught). In our models, the presence/absence component predicts the probability (p, ranging from 0-1) of a longline catching zero fish of a given species and the positive count component predicts the non-zero number of fish caught when the longline catches the given species (mu, > 0). The hurdle model then combines these two components to predict the catch response (in numbers of fish) of a given species:

$$Response = mu * (1 - p)$$

We used a binomial error family for the presence/absence component and a zero-truncated negative binomial error family for the positive count component. This hurdle model approach has the flexibility to properly account for the high proportions of zero catches (i.e., gear deployments that caught no fish) and overdispersion (i.e., high variability in the numbers of fish caught) that often characterize such data (Fig. S20).

For each species, we first constructed a base model that excluded eddy-related terms but included the following higher-order environmental and fishing-related terms in both the presence/absence and positive count components of the hurdle GLMMs; interannual variation (factor of year; 1995 – 2017), intraannual variation (factor for quarter; January – March [Quarter 1], April – June [Quarter 2], July – September [Quarter 3], October – December [Quarter 4]), large-scale spatial variation (factor for quadrant; 25 – 40°N & 180 – 155°W [Quadrant 1], 10 – 25°N & 180 – 155°W [Quadrant 2], 25 – 40°N & 155 – 130°W [Quadrant 3], 10 – 25°N & 155 – 130°W [Quadrant 4]), spatiotemporal variation (interaction of factors for quarter and quadrant), fishing depth (proxied by a factor for hooks per float; 15 – 24 [shallower], 25 – 29 [intermediate], >= 30 [deeper]), gear quantity (linear term of log-transformed number of hooks), and fisher behavior (random term for confidential, vessel-specific code). These terms were chosen based on previous expert standardizations of federal observer data from this fishery [e.g., 55, 56] and reflect environmental variation around major boundaries (e.g., the vertical habitat and deep scattering layer community composition change from the

northern portion of the subtropical gyre $> 25°$N to the southern portion $< 25°$N, [57]) as well as variable fisher behavior. We did not include further interactions among terms (or finer-resolution levels within factor terms) given their propensity to yield factor-factor combinations with unresolved estimates, especially in the positive count component of the models for species with fewer positive longline sets. While catch-effort standardization often entails exhaustive testing of all possible terms and interactions to yield the best formulation unique to each species, we used the same base formulation for all species so as to yield consistently standardized and comparable results across the predator community. This enabled us to conservatively compare a standardized base model without the eddy-related terms of interest against more complex configurations that added eddy-related terms in the presence/absence component, the positive count component, or both components in the hurdle GLMM for each species. Eddy-related terms included the eddy type (factor for polarity; anticyclonic, cyclonic), eddy zone (factor for normalized distance from eddy center; $0.0 - 0.5R$ [inner core], $0.5 - 1.0R$ [outer core], $1.0 - 1.5R$ [inner periphery], $1.5 - 2.0R$ [outer periphery]), and the eddy dynamics subregion (factor for eddy kinetic energy; $< 150\ cm^2s^{-2}$ [low EKE], $> 150\ cm^2s^{-2}$ [high EKE]). It is important to note that our exclusion of data from areas devoid of eddy influence (i.e., beyond eddy peripheries) in this analysis prevented the perfect collinearity issue that would arise from our model-standardization terms for factors 'eddy type' and 'eddy zone' if forced to include additional levels of 'neither polarity' and '$> 2.0R$ [beyond eddy influence]', respectively.

Each hurdle GLMM contained both the presence/absence component and the positive count component. For each model formulation, each of the two components in the model was tested as one of three configurations; (1) base model with no eddy effects, (2) base model plus gyre-wide eddy effects, and (3) base model plus EKE subregion-specific eddy effects. Thus, nine possible model configurations were tested for each species (3 permutations for each of 2 model components), in addition to the null model configuration used as a control, resulting in ten total GLMM configurations per species (Table S2). In the following equations, the model notation "*" indicates the inclusion of main and interaction effects from the immediately adjacent variables (e.g., a*b = a + b + a:b), "log(...)" indicates a natural logarithm transformation of the specified variable, "(1|...)" indicates a random group intercept, and "/" indicates a nested interaction of the variable(s) (and any interaction thereof) on the immediate left of the symbol with the variable on the immediate right but exclusion of the main effect solely from the variable on the right (e.g., a/b = a + a:b). The base model configuration (Eq. 1) suggests eddies have no effect on pelagic predator catch:

$$Component \sim Year + Quarter * Quadrant + Fishing\ Depth + log(Number\ of\ Hooks) + (1|Code) \quad (1)$$

The gyre-wide configuration (Eq. 2) suggests there are eddy-related effects on pelagic predator catch that are constant across the North Pacific Subtropical Gyre, and was structured to include the main effects of eddy type and eddy zone plus their interaction:

$$\begin{aligned} Component \sim Year + Quarter * Quadrant + Fishing\ Depth + log(Number\ of\ Hooks) + (1|Code) \\ + Eddy\ Type * Eddy\ Zone \end{aligned} \tag{2}$$

The EKE subregion-specific configuration (Eq. 3) suggests there are eddy-related effects on pelagic predator catch that are different across the low and high EKE subregions of the North Pacific Subtropical Gyre, and this model was structured to include the main effects of eddy type and eddy zone, the interaction of eddy type and eddy zone, and the nested interaction of those terms with the eddy dynamics subregion. No main effect for the eddy dynamics subregion is included since large-scale spatial variation is already accounted for by the factor for quadrant included among the base terms:

$$\begin{aligned} Component \sim Year + Quarter * Quadrant + Fishing\ Depth + log(Number\ of\ Hooks) + (1|Code) \\ + (Eddy\ Type * Eddy\ Zone)/Eddy\ Dynamics\ Subregion \end{aligned} \tag{3}$$

Given the three potential configurations for each of the presence/absence and positive count components, nine alternative hurdle GLMM formulations per species were compared to the species-specific null model to identify the best-fit model. Model selection was done with Akaike's Information Criterion (AIC) and the derived metric of AIC weight; for a group of models being compared, the AIC weight of all models sums to 1 and the model with the highest AIC weight is the best-fit. However, in instances of competing models (with none individually exhibiting an AIC weight ≥ 0.8), the most parsimonious supported model (with AIC weight ≥ 0.2) was conservatively selected (Table S2). Validation of the best-fit model for each species included inspection of quantile-quantile (Q-Q), residual vs prediction, and residual vs predictor plots.

Mean effect estimate results from the best-fit hurdle GLMM for each species were presented as odds (presence/absence component) and rate (positive count component) ratios of the catch metrics in a given zone of an anticyclonic eddy relative to those in the corresponding zone of a cyclonic eddy (either gyre-wide or within a specific eddy dynamics subregion, depending on the formulation of the best-fit model). The 95% confidence intervals for these ratios were estimated using the delta method, which enables estimation of the

error of an estimate that is itself calculated from multiple estimates, each with their own error and covariance among them. A given odds or rate ratio was determined as statistically significant if its 95% confidence interval did not encompass 1 (the null value representing no difference).

Similarly, the estimated marginal mean responses of the best-fit hurdle GLMM for each species were computed to determine the model-predicted catch of the "average" longline set by eddy polarity, eddy zone, and eddy dynamics subregion. Computation of the estimated marginal means was done for the presence/absence and positive count component of each hurdle GLMM; the expected probability of a non-zero longline set (i.e., presence) was multiplied by the expected positive number of fish (i.e., positive count) to yield the catch response. These estimated marginal means were balanced across the lone continuous predictor (held to its average value) and all unique factor predictor combinations to prevent potential bias from the unbalanced nature of the underlying dataset (e.g., fishing effort was not distributed equally in space and time). Furthermore, the estimated marginal means were bias-adjusted for the additive random effect (fisher behavior) present in all hurdle GLMMs in this study; the bias-adjustment of the presence/absence and positive count components was informed by the standard deviation of the random effect estimated in the respective component of the model (failure to do this would result in underestimated marginal mean values). These species-specific predicted catches were then summed across all 14 predator taxa included in this study to determine the overall predicted catch of the "average" longline set in a given eddy polarity, eddy zone, and eddy dynamics subregion.

Model-standardization, validation, estimation of odds and rate ratio confidence intervals, and estimation of balanced marginal means were conducted with the `glmmTMB` [58], `DHARMa` [59], `msm` [60], `lme4` [61], and `emmeans` [62] packages in R version 3.6.3 [63].

2.5 Model-Standardization of Logbook Data: Complementary Analysis with Non-Eddy Baseline

To further contextualize the preceding analysis from within areas of eddy impact (i.e., within eddy cores and peripheries), we conducted a complementary catch-effort standardization analysis comparing amongst the cores of eddies of both polarities and areas devoid of eddy influence (i.e., beyond eddy peripheries). This comparison, which excluded eddy peripheries, was designed to formally provide a non-eddy baseline against which to compare catch metrics from inside anticyclones and cyclones. Eddy peripheries were excluded because they do not necessarily reflect the biophysical conditions inside eddies and can experience impacts from eddies making them dissimilar from more distant areas fully devoid of eddy influence. From the filtered logbook dataset of 318,200 longline sets, this complementary analysis used 182,775 longline sets that occurred

within the cores of eddies (n = 84,609 sets in 3,587 unique eddies representing 53,970 daily eddy realizations) or in areas devoid of eddy influence (n = 98,166 sets) and caught a combined total of 5,370,203 fish across the 14 aforementioned pelagic predator taxa. Note that the blue shark model utilized 146 longline sets less than all other species due to non-reporting of those particular catches.

Using the same methodological approach as the eddy-centric analysis, we identified and quantified the potential for eddies to modulate the catch of pelagic fishes by building models with and without eddy-related terms of varying complexity that also standardized for variability in catch arising from higher-order environmental processes and different fishing methodologies. To achieve this standardization, we used hurdle generalized linear mixed models (GLMMs) that modeled catch (in numbers of fish) as the response. We first constructed a base model for each species that excluded eddy-related terms but included the following higher-order environmental and fishing-related terms in both the presence/absence and positive count components of the hurdle GLMMs; interannual variation (factor of year; 1995 – 2017), intraannual variation (factor for quarter; January – March [Quarter 1], April – June [Quarter 2], July – September [Quarter 3], October – December [Quarter 4]), large-scale spatial variation (factor for quadrant; 25 – 40°N & 180 – 155°W [Quadrant 1], 10 – 25°N & 180 – 155°W [Quadrant 2], 25 – 40°N & 155 – 130°W [Quadrant 3], 10 – 25°N & 155 – 130°W [Quadrant 4]), spatiotemporal variation (interaction of factors for quarter and quadrant), fishing depth (proxied by a factor for hooks per float; 15 – 24 [shallower], 25 – 29 [intermediate], >= 30 [deeper]), gear quantity (linear term of log-transformed number of hooks), and fisher behavior (random term for confidential, vessel-specific code). While catch-effort standardization often entails exhaustive testing of all possible terms and interactions to yield the best formulation unique to each species, we used the same base formulation for all species so as to yield consistently standardized data across the predator community. This enabled us to conservatively compare a standardized base model without the eddy-related terms of interest against more complex configurations that added eddy-related terms in the presence/absence component, the positive count component, or both components in the hurdle GLMM for each species. Eddy-related terms included the eddy category (factor for location; anticyclone core [0.0 – 1.0R], cyclone core [0.0 – 1.0R], non-eddy [> 2.0R]) and the eddy dynamics subregion (factor for eddy kinetic energy; < 150 cm^2s^{-2} [low EKE], > 150 cm^2s^{-2} [high EKE]). It is important to note that, in this complementary analysis, the eddy cores were not further differentiated into inner and outer zones.

Each hurdle GLMM contained both the presence/absence component and the positive count component. For each model formulation, each of the two components in the model was tested as one of three configurations; (1) base model with no eddy effects, (2) base model plus gyre-wide eddy effects, and (3) base model plus EKE subregion-specific eddy effects. Thus, nine possible model configurations were tested for each species (3

permutations for each of 2 model components), in addition to the null model configuration used as a control, resulting in ten total GLMM configurations per species (Table S6). In the following equations, the model notation "*" indicates the inclusion of main and interaction effects from the immediately adjacent variables (e.g., a*b = a + b + a:b), "log(...)" indicates a natural logarithm transformation of the specified variable, "(1|...)" indicates a random group intercept, and "/" indicates a nested interaction of the variable on the immediate left of the symbol with the variable on the immediate right but exclusion of the main effect solely from the variable on the right (e.g., a/b = a + a:b). The base model configuration (Eq. 4) suggests eddies have no effect on pelagic predator catch:

$$Component \sim Year + Quarter * Quadrant + Fishing\ Depth + log(Number\ of\ Hooks) + (1|Code) \quad (4)$$

The gyre-wide configuration (Eq. 5) suggests there are eddy-related effects on pelagic predator catch that are constant across the North Pacific Subtropical Gyre, and was structured to include the main effect of eddy category:

$$\begin{aligned} Component \sim Year + Quarter * Quadrant + Fishing\ Depth + log(Number\ of\ Hooks) + (1|Code) \\ + Eddy\ Category \end{aligned} \quad (5)$$

The EKE subregion-specific configuration (Eq. 6) suggests there are eddy-related effects on pelagic predator catch that are different across the low and high EKE subregions of the North Pacific Subtropical Gyre, and this model was structured to include the main effect of eddy category and its nested interaction with the eddy dynamics subregion. No main effect for the eddy dynamics subregion is included since large-scale spatial variation is already accounted for by the factor for quadrant included among the base terms:

$$\begin{aligned} Component \sim Year + Quarter * Quadrant + Fishing\ Depth + log(Number\ of\ Hooks) + (1|Code) \\ + Eddy\ Category/Eddy\ Dynamics\ Subregion \end{aligned} \quad (6)$$

Given the three potential configurations for each of the presence/absence and positive count components, nine alternative hurdle GLMM formulations per species were compared to identify the best-fit model. Model selection was done with Akaike's Information Criterion (AIC) and the derived metric of AIC weight; for a group of models being compared, the AIC weight of all models sums to 1 and the model with the highest

AIC weight is the best-fit. However, in instances of competing models (with none individually exhibiting an AIC weight ≥ 0.8), the most parsimonious supported model (with AIC weight ≥ 0.2) was conservatively selected (Table S2). Validation of the best-fit model for each species included inspection of quantile-quantile (Q-Q), residual vs prediction, and residual vs predictor plots.

Mean effect estimate results from the best-fit hurdle GLMM for each species were presented as odds (presence/absence component) and rate (positive count component) ratios of the catch metrics in 1) a cyclone core relative to those in a non-eddy area, 2) an anticyclone core relative to those in a non-eddy area, and 3) an anticyclone core relative to those in a cyclone core (either gyre-wide or within a specific eddy dynamics subregion, depending on the formulation of the best-fit model). The 95% confidence intervals for these ratios were estimated using the delta method. A given odds or rate ratio was determined as statistically significant if its 95% confidence interval did not encompass 1 (the null value representing no difference).

Model-standardization, validation, and estimation of odds and rate ratio confidence intervals were conducted with the `glmmTMB` [58], `DHARMa` [59], and `msm` [60] packages in R version 3.6.3 [63].

2.6 Eddy Vertical Structure Composite Averages

Composite averages of eddy vertical structure were computed using Argo float profiles co-located to the center of eddies. Delayed-time Argo profiles that underwent expert quality control were downloaded from the NOAA National Center for Environmental Information's Argo Data Repository (https://www.nodc.noaa.gov/argo/floats_data.htm). The distance from eddy center normalized by the radius R of the nearest eddy was used to compute radial composite averages for anticyclones and cyclones. For clarity in presentation, the composites were mirrored across the origin (eddy center) and smoothed using half-power cutoffs equivalent to a running mean span of $0.2R$ in normalized distance from eddy center and 40 m in depth.

3 Results

3.1 Eddy Characteristics

The North Pacific Subtropical Gyre contains mesoscale eddies that vary in amplitude, radius, rotational velocity, and age (Fig. S21, Table S8). When isolating eddies that were co-located to the fishery data from all the mesoscale eddies identified and tracked in the region, no significant difference was detected in eddy intensity, which integrates eddy amplitude and radius (two-sample Kolmogorov-Smirnov goodness-of-fit hypothesis tests – anticyclones, $D = 0.11$, $p = 0.99$; cyclones, $D = 0.11$, $p = 0.99$). As a result, we used all observed eddies in the study region to conduct our analysis of eddy characteristics.

Eddies of both polarities in the high EKE subregion were typically more energetic (with larger amplitude and faster rotation) than those in the low EKE subregion (Fig. S21a,c), and there was a greater proportion of large eddies in the former (Fig. S21b). In the high EKE subregion, a greater portion of highly-energetic eddies were cyclonic, which was not observed in the low EKE subregion (Fig. S21a,c). Eddies of both polarities in the age range of ∼200 – 350 days were proportionally more common in the low than high EKE subregion (Fig. S21d).

3.2 Eddy-Centric Analysis

Given the extensive coverage of this analysis in the main manuscript, only the model validation results are detailed here. The deviance explained of the selected model for each species (relative to the null model without fixed nor random effects) was as follows: albacore (12.1%), bigeye tuna (2.9%), skipjack tuna (6.8%), yellowfin tuna (7.5%), blue marlin (8.1%), striped marlin (7.3%), shortbill spearfish (5.6%), swordfish (6.1%), blue shark (6.8%), dolphinfish (6.4%), escolar (9.0%), opah (8.4%), pomfret (4.8%), and wahoo (8.6%). This suggests that catch-effort standardization reduced the effects of potentially confounding factors but unexplained variation remains (such as that which could be explained by factors not available in the logbook dataset). Model diagnostics (Fig. S22, S23, S24, S25) from the simulation approach of `DHARMa` [59] relied on standardized residuals scaled between values of 0 and 1, and predictions that multiplied the expected probability of a non-zero longline set (that caught fish of a given species) by the expected positive number of fish to yield the catch response. All species' models exhibited reasonable Q-Q plots but that of blue shark showed slight deviation from the expected distribution; in these Q-Q plots, which compare the distribution of the catch data to that of the statistical model of those data, correct model specification is indicated by the black points overlapping the red diagonal. Residual versus prediction plots (ideally with the red spline being uniform in the Y-direction around the value of 0.50) also suggested widespread model validity; these plots are capable of identifying model issues that do not necessarily appear in Q-Q plots. In the residual versus prediction plots, simulation outliers (red circles, standardized residuals of value 0 or 1) were largely present where the models underpredicted catches relative to those observed; this is not unexpected for such highly variable catch data in which extremely large catch events are less common and difficult to predict. However, only the model for bigeye tuna yielded a significantly, albeit minimally, higher frequency of outliers than expected (+0.15%). Both this increase in outliers and the relatively low deviance explained of the bigeye tuna model are at least partially attributable to the markedly high proportion of positive sets for this species (92.5%), which makes it difficult to discern when absences should occur. We note that, in the residual versus prediction plots, some species' models exhibited a tendency for underprediction of the larger catches (red

spline above 0.50 on the far right side of the X-axis - e.g., dolphinfish, opah, pomfret). In contrast, only the models for blue shark and escolar exhibited a tendency for both overprediction of smaller catches (red line below 0.50 to the left) and underprediction of larger catches (red line above 0.50 to the right). The relatively poorer diagnostics of the blue shark and escolar models may be due to these grouped species categories being either wholly or partially comprised of non-commercialized species that are not counted as accurately due to them not being landed. Some captains count all shark species as 'blue shark' (Jon Brodziak, NOAA PIFSC, pers. comm.), none of which are harvested for sale. Similarly, oilfish (*Ruvettus pretiosus*) are included in the 'escolar' group but are not harvested for sale whereas escolar (*Lepidocybium flavobrunneum*) are landed. This strongly contrasts with the other predator species (or groups thereof) that are harvested for sale whether or not they are directly targeted. Regardless of a species' commercialization, misprediction of some catches may be at least partially attributable to 1) missing predictor variables, or interactions thereof, including those not available in the logbook dataset that are known to further influence catch patterns and/or 2) coarse levels within factor predictor variables that preclude more nuanced effect estimates. Residual versus predictor plots (not shown) suggested some deviation from uniformity with respect to gear quantity (linear term of log-transformed number of hooks) for certain species; however, extensive testing revealed that excluding this term would yield models with worse diagnostics (less valid), and alternative formulations (as an offset or as an explanatory variable on the original scale) yielded worse diagnostics or failed to converge. Given that catch (in numbers of fish) is the response in our models, it is necessary to account for such measures of effort [22]. The number of hooks is the best available metric of effort in the logbook dataset, and the log-transformed version of this term (as we use it) has also been used in recent expert standardizations of observer data from the fishery [56].

3.3 Complementary Analysis with Non-Eddy Baseline

Catch standardization models accounting for mesoscale eddies exhibited the best fit to the fishery data for all 14 pelagic predators tested (Table S6). In the high EKE subregion, catch odds (rates) were significantly greater in anticyclones than non-eddy areas for 10 (9) species, significantly greater in anticyclones than cyclones for 11 (10) species, and significantly greater in cyclones than non-eddy areas for 1 (1) species; in contrast, catch odds (rates) were significantly lower in anticyclones than non-eddy areas for 2 (2) species, significantly lower in anticyclones than cyclones for 1 (2) species, and significantly lower in cyclones than non-eddy areas for 8 (6) species (Fig. S17). In the low EKE subregion, catch odds (rates) were significantly greater in anticyclones than non-eddy areas for 7 (7) species, significantly greater in anticyclones than cyclones for 10 (11) species, and significantly greater in cyclones than non-eddy areas for 2 (1) species; in contrast,

catch odds (rates) were significantly lower in anticyclones than non-eddy areas for 0 (0) species, significantly lower in anticyclones than cyclones for 0 (0) species, and significantly lower in cyclones than non-eddy areas for 8 (9) species (Fig. S17). The pelagic predators that exhibited significantly greater catch odds, rates, or both in anticyclones than non-eddy areas included albacore, striped marlin, blue marlin, spearfish, dolphinfish, wahoo, and escolar in the low and high EKE subregions, bigeye tuna and blue shark in only the low EKE subregion, and yellowfin tuna, skipjack tuna, swordfish, and pomfret in only the high EKE subregion (Fig. S17). In contrast, the pelagic predators that exhibited significantly greater catch odds, rates, or both in cyclones than non-eddy areas included dolphinfish in the low and high EKE subregions, and blue shark and opah in only the low EKE subregion (Fig. S17). The only species that, for a given catch metric, exhibited a reversal from significantly lower to significantly higher (or vice-versa) in anticyclones versus non-eddy areas were bigeye tuna and blue shark (i.e., lower catch rates in anticyclones in high EKE but higher in anticyclones in low EKE); however, bigeye tuna catch rates were always significantly higher in anticyclones than cyclones (Fig. S17). In contrast, the only species that, for a given catch metric, exhibited a reversal from significantly lower to significantly higher (or vice-versa) in cyclones versus non-eddy areas was dolphinfish (i.e., higher catch rates in cyclones in high EKE but lower in cyclones in low EKE) (Fig. S17). Averaging across species-specific estimates (and depending on the underlying EKE subregion), the mean catch odds (rates) were 6-7 (5-6)% higher in anticyclones than non-eddy areas, 5-8 (3-6)% higher in non-eddy areas than cyclones, and 13-16 (10-13)% higher in anticyclones than cyclones (Table S7).

The deviance explained of the selected model for each species (relative to the null model without fixed nor random effects) was as follows: albacore (10.8%), bigeye tuna (2.9%), skipjack tuna (6.1%), yellowfin tuna (6.6%), blue marlin (8.0%), striped marlin (7.0%), shortbill spearfish (5.4%), swordfish (5.8%), blue shark (6.7%), dolphinfish (6.7%), escolar (9.1%), opah (8.4%), pomfret (5.3%), and wahoo (8.7%). This suggests that catch-effort standardization reduced the effects of potentially confounding factors but unexplained variation remains (such as that which could be explained by factors not available in the logbook dataset). Model diagnostics (Fig. S26, S27, S28, S29) from the simulation approach of `DHARMa` [59] relied on standardized residuals scaled between values of 0 and 1, and predictions that multiplied the expected probability of a non-zero longline set (that caught fish of a given species) by the expected positive number of fish to yield the catch response. All species' models exhibited reasonable Q-Q plots but that of blue shark showed slight deviation from the expected distribution. Residual versus prediction plots also suggested widespread model validity. In the residual versus prediction plots, simulation outliers (red circles, standardized residuals of value 0 or 1) were largely present where the models underpredicted catches relative to those observed; this is not unexpected for such highly variable catch data in which extremely large catch events are rare and difficult

to predict. However, only the model for bigeye tuna yielded a significantly, albeit minimally, higher frequency of outliers than expected (+0.12%). Both this increase in outliers and the relatively low deviance explained of the bigeye tuna model are at least partially attributable to the markedly high proportion of positive sets for this species (92.5%), which makes it difficult to discern when absences should occur. We note that, in the residual versus prediction plots, some species' models exhibited a tendency for underprediction of the larger catches (red spline above 0.50 on the far right side of the X-axis - e.g., dolphinfish, opah, pomfret). In contrast, only the models for blue shark and escolar exhibited a tendency for both overprediction of smaller catches (red line below 0.50 to the left) and underprediction of larger catches (red line above 0.50 to the right), which may be due to these grouped species categories being wholly or partially comprised of non-commercialized species. Residual versus predictor plots (not shown) suggested some deviation from uniformity with respect to gear quantity (linear term of log-transformed number of hooks) for certain species. Given that catch (in numbers of fish) is the response in our models, it is necessary to account for such measures of effort [22]. The number of hooks is the best available metric of effort in the logbook dataset, and the log-transformed version of this term (as we use it) has also been used in recent expert standardizations of observer data from the fishery [56].

4 Tables

Table S1: Summary of the population assessment and catch data co-located to eddies of the 14 pelagic predators included in this study. Population status and trend (as of September 2021) come from the global assessment and listing by the International Union for the Conservation of Nature (IUCN) and the regional assessment and listing by the Western & Central Pacific Fisheries Commission (WCPFC). Positive sets represent the number of longline sets that caught the focal predator, and number captured represents the summed number of individuals of that focal predator captured across those positive sets. *Scientific name listed is of the predominant species in grouped species categories.

Pelagic Predator	Scientific Name	IUCN	WCPFC	Positive Sets	Number Captured
Albacore	*Thunnus alalunga*	Near Threatened Decreasing	Not Overfished Not Evaluated	63,983	380,336
Bigeye Tuna	*Thunnus obesus*	Vulnerable Decreasing	Not Overfished No Overfishing	203,529	2,023,659
Yellowfin Tuna	*Thunnus albacares*	Near Threatened Decreasing	Not Overfished No Overfishing	95,513	329,271
Skipjack Tuna	*Katsuwonus pelamis*	Least Concern Stable	Not Overfished No Overfishing	71,690	283,207
Striped Marlin	*Kajikia audax*	Near Threatened Decreasing	Overfished Overfishing	85,420	192,275
Blue Marlin	*Makaira nigricans*	Vulnerable Decreasing	Not Overfished No Overfishing	40,996	65,514
Shortbill Spearfish	*Tetrapturus angustirostris*	Data Deficient Unknown	Not Evaluated Not Evaluated	89,646	191,633
Swordfish	*Xiphias gladius*	Least Concern Decreasing	Not Overfished No Overfishing	35,250	48,263
Blue Shark	*Prionace glauca**	Near Threatened Decreasing	Not Overfished No Overfishing	158,159	703,505
Wahoo	*Acanthocybium solandri*	Least Concern Stable	Not Evaluated Not Evaluated	94,394	199,521
Dolphinfish	*Coryphaena hippurus**	Least Concern Stable	Not Evaluated Not Evaluated	143,581	822,076
Opah	*Lampris* spp.	Least Concern Unknown	Not Evaluated Not Evaluated	102,762	244,220
Pomfret	*Taractichthys steindachneri**	Not Evaluated Not Evaluated	Not Evaluated Not Evaluated	143,538	630,434
Escolar	*Lepidocybium flavobrunneum**	Least Concern Unknown	Not Evaluated Not Evaluated	106,663	294,904

Table S2: Eddy-Centric Analysis: Hurdle model selection results for each of the 14 pelagic predators, including the configuration, the difference in AIC relative to the model with the lowest score (dAIC), and AIC weight (AICw). Model configuration is specified as Eq. # for Presence/Absence component|Eq. # for Positive Count component. For example, 2|1 indicates the gyre-wide configuration (Eq. 2) was used for the presence-absence component and the base model configuration (Eq. 1) was used for the positive count component. The null models included for comparison exclude all fixed and random effects.

		Presence/Absence			**Positive Count**					
Predator	**Config**	**Base**	**Gyre**	**Subregion**	**Base**	**Gyre**	**Subregion**	**dAIC**	**AICw**	**Selected**
Albacore	Null							71097.0	0	
	1|1	x			x			1472	0	
	2|1		x		x			846.8	0	
	1|2	x				x		1268.5	0	
	2|2		x			x		643.3	0	
	1|3	x					x	1143.4	0	
	2|3		x				x	518.2	0	
	3|1			x	x			328.6	0	
	3|2			x		x		125.1	0	
	3|3			x			x	0	1	*
Bigeye Tuna	Null							41545.8	0	
	1|1	x			x			4361.3	0	
	2|1		x		x			4296.4	0	
	1|2	x				x		4271.1	0	
	2|2		x			x		4206.2	0	
	1|3	x					x	1960.3	0	
	2|3		x				x	1895.4	0	
	3|1			x	x			2400.9	0	
	3|2			x		x		2310.8	0	
	3|3			x			x	0	1	*

continued

		Presence/Absence			Positive Count					
Predator	**Config**	**Base**	**Gyre**	**Subregion**	**Base**	**Gyre**	**Subregion**	**dAIC**	**AICw**	**Selected**
Yellowfin Tuna	Null							51178.5	0	
	1|1	x			x			152.7	0	
	2|1		x		x			49.3	0	
	1|2	x				x		117	0	
	2|2		x			x		13.7	0	
	1|3	x					x	129	0	
	2|3		x				x	25.6	0	
	3|1			x	x			35.7	0	
	3|2			x		x		0	1	*
	3|3			x			x	12	0	
Skipjack Tuna	Null							40287.2	0	
	1|1	x			x			191.8	0	
	2|1		x		x			90.9	0	
	1|2	x				x		178.6	0	
	2|2		x			x		77.8	0	
	1|3	x					x	124.3	0	
	2|3		x				x	23.4	0	
	3|1			x	x			67.5	0	
	3|2			x		x		54.4	0	
	3|3			x			x	0	1	*

continued

		Presence/Absence			Positive Count					
Predator	**Config**	**Base**	**Gyre**	**Subregion**	**Base**	**Gyre**	**Subregion**	**dAIC**	**AICw**	**Selected**
Striped Marlin	Null							40501.8	0	
	1|1	x			x			1947.3	0	
	2|1		x		x			1891.4	0	
	1|2	x				x		1930.7	0	
	2|2		x			x		1874.8	0	
	1|3	x					x	1118.2	0	
	2|3		x				x	1062.3	0	
	3|1			x	x			829.1	0	
	3|2			x		x		812.5	0	
	3|3			x			x	0	1	*
Blue Marlin	Null							23809.9	0	
	1|1	x			x			398.8	0	
	2|1		x		x			327.2	0	
	1|2	x				x		381.5	0	
	2|2		x			x		309.9	0	
	1|3	x					x	385.4	0	
	2|3		x				x	313.8	0	
	3|1			x	x			17.3	0	
	3|2			x		x		0	0.88	*
	3|3			x			x	3.9	0.12	

continued

		Presence/Absence			Positive Count					
Predator	**Config**	**Base**	**Gyre**	**Subregion**	**Base**	**Gyre**	**Subregion**	**dAIC**	**AICw**	**Selected**
Shortbill Spearfish	Null							31357.8	0	
	1|1	x			x			632.3	0	
	2|1		x		x			465.9	0	
	1|2	x				x		561.2	0	
	2|2		x			x		394.8	0	
	1|3	x					x	330.3	0	
	2|3		x				x	163.9	0	
	3|1			x	x			302	0	
	3|2			x		x		230.9	0	
	3|3			x			x	0	1	*
Swordfish	Null							14956.5	0	
	1|1	x			x			25.8	0	
	2|1		x		x			7.2	0.02	
	1|2	x				x		24.8	0	
	2|2		x			x		6.3	0.02	
	1|3	x					x	30.3	0	
	2|3		x				x	11.7	0	
	3|1			x	x			0.9	0.36	*
	3|2			x		x		0	0.56	
	3|3			x			x	5.4	0.04	

continued

		Presence/Absence			Positive Count					
Predator	**Config**	**Base**	**Gyre**	**Subregion**	**Base**	**Gyre**	**Subregion**	**dAIC**	**AICw**	**Selected**
Blue Shark	Null							68501.3	0	
	1|1	x			x			31.2	0	
	2|1		x		x			34.2	0	
	1|2	x				x		17.5	0	
	2|2		x			x		20.4	0	
	1|3	x					x	1.8	0.27	*
	2|3		x				x	4.7	0.06	
	3|1			x	x			29.5	0	
	3|2			x		x		15.7	0	
	3|3			x			x	0	0.66	
Wahoo	Null							49089.4	0	
	1|1	x			x			2171.8	0	
	2|1		x		x			1991.7	0	
	1|2	x				x		2127.3	0	
	2|2		x			x		1947.2	0	
	1|3	x					x	1761.5	0	
	2|3		x				x	1581.4	0	
	3|1			x	x			410.3	0	
	3|2			x		x		365.8	0	
	3|3			x			x	0	1	*

continued

		Presence/Absence			Positive Count					
Predator	**Config**	**Base**	**Gyre**	**Subregion**	**Base**	**Gyre**	**Subregion**	**dAIC**	**AICw**	**Selected**
Dolphinfish	Null							66115.5	0	
	1|1	x			x			398.3	0	
	2|1		x		x			399.8	0	
	1|2	x				x		384.9	0	
	2|2		x			x		386.5	0	
	1|3	x					x	3.6	0.13	
	2|3		x				x	5.1	0.06	
	3|1			x	x			394.7	0	
	3|2			x		x		381.3	0	
	3|3			x			x	0	0.8	*
Opah	Null							53268.6	0	
	1|1	x			x			120.5	0	
	2|1		x		x			95.5	0	
	1|2	x				x		125.3	0	
	2|2		x			x		100.3	0	
	1|3	x					x	121.8	0	
	2|3		x				x	96.9	0	
	3|1			x	x			0	0.63	*
	3|2			x		x		4.8	0.06	
	3|3			x			x	1.4	0.32	

continued

		Presence/Absence			Positive Count					
Predator	**Config**	**Base**	**Gyre**	**Subregion**	**Base**	**Gyre**	**Subregion**	**dAIC**	**AICw**	**Selected**
Pomfret	Null							45698.2	0	
	1|1	x			x			8984.7	0	
	2|1		x		x			8813.9	0	
	1|2	x				x		8559.6	0	
	2|2		x			x		8388.8	0	
	1|3	x					x	2262.3	0	
	2|3		x				x	2091.5	0	
	3|1			x	x			6722.4	0	
	3|2			x		x		6297.3	0	
	3|3			x			x	0	1	*
Escolar	Null							61790.2	0	
	1|1	x			x			609.1	0	
	2|1		x		x			359.8	0	
	1|2	x				x		264.1	0	
	2|2		x			x		14.7	0	
	1|3	x					x	249.4	0	
	2|3		x				x	0	0.99	*
	3|1			x	x			368.4	0	
	3|2			x		x		23.3	0	
	3|3			x			x	8.6	0.01	

Table S3: Eddy-Centric Analysis: Summary of model-estimated catch odds and rate ratios (anticyclone/cyclone) across species. Results are shown within each EKE subregion and across them.

EKE	Ratio	Eddy Zone	Min	1st Qu.	Median	Mean	3rd Qu.	Max	N
High	Odds	Core - Inner	0.93	1.11	1.17	1.18	1.21	1.68	14
		Core - Outer	0.89	1.06	1.12	1.12	1.19	1.32	14
		Periphery - Inner	0.98	1.04	1.08	1.07	1.10	1.11	14
		Periphery - Outer	0.95	1.02	1.04	1.04	1.07	1.13	14
	Rate	Core - Inner	0.93	1.02	1.12	1.15	1.28	1.45	14
		Core - Outer	0.96	1.01	1.06	1.08	1.15	1.23	14
		Periphery - Inner	0.98	1.02	1.03	1.04	1.07	1.12	14
		Periphery - Outer	0.99	1.00	1.01	1.02	1.05	1.08	14
Low	Odds	Core - Inner	1.00	1.08	1.19	1.21	1.24	1.79	14
		Core - Outer	0.95	1.06	1.10	1.15	1.21	1.67	14
		Periphery - Inner	0.96	1.02	1.05	1.05	1.08	1.14	14
		Periphery - Outer	0.83	0.97	0.99	0.99	1.01	1.06	14
	Rate	Core - Inner	0.99	1.02	1.10	1.16	1.20	1.83	14
		Core - Outer	1.00	1.04	1.07	1.11	1.17	1.43	14
		Periphery - Inner	0.97	1.01	1.03	1.05	1.08	1.25	14
		Periphery - Outer	0.95	0.97	1.00	1.01	1.02	1.11	14
Both	Odds	Core - Inner	0.93	1.09	1.18	1.20	1.22	1.79	28
		Core - Outer	0.89	1.05	1.12	1.13	1.21	1.67	28
		Periphery - Inner	0.96	1.03	1.06	1.06	1.10	1.14	28
		Periphery - Outer	0.83	0.99	1.01	1.02	1.05	1.13	28
	Rate	Core - Inner	0.93	1.01	1.11	1.15	1.24	1.83	28
		Core - Outer	0.96	1.02	1.06	1.09	1.16	1.43	28
		Periphery - Inner	0.97	1.01	1.03	1.05	1.08	1.25	28
		Periphery - Outer	0.95	0.99	1.01	1.02	1.04	1.11	28

Table S4: Eddy-Centric Analysis: Ratios (anticyclone/cyclone) of catch summed across the 14 pelagic predator species for the average longline set. Predicted catch responses from each of the species-specific models were summed to produce the overall catch response by eddy polarity, eddy zone, and eddy dynamics subregion.

EKE	Eddy Zone	Ratio
High	Core - Inner	1.12
	Core - Outer	1.07
	Periphery - Inner	1.04
	Periphery - Outer	1.02
Low	Core - Inner	1.11
	Core - Outer	1.09
	Periphery - Inner	1.05
	Periphery - Outer	1.00

Table S5: Eddy-Centric Analysis: Summary of species-specific proportional contributions (%) to the overall catch response predicted for the average longline set in the 16 unique combinations of eddy polarity, eddy zone, and eddy dynamics subregion.

Predator	Min	1st Qu.	Median	Mean	3rd Qu.	Max
Albacore	1.41	2.45	3.43	3.42	4.08	5.85
Bigeye Tuna	42.83	43.99	45.95	46.23	48.47	50.95
Yellowfin Tuna	1.25	1.33	1.50	1.50	1.68	1.85
Skipjack Tuna	1.77	1.90	2.17	2.28	2.68	2.89
Striped Marlin	1.43	1.50	2.34	2.39	3.27	3.47
Blue Marlin	0.18	0.20	0.21	0.21	0.22	0.24
Shortbill Spearfish	1.42	1.48	1.83	1.92	2.30	2.67
Swordfish	0.06	0.06	0.07	0.07	0.07	0.08
Blue Shark	10.57	11.23	12.07	12.30	13.22	14.69
Wahoo	1.34	1.42	1.67	1.67	1.88	2.04
Dolphinfish	11.80	12.26	12.55	12.64	12.92	14.14
Opah	3.58	3.83	4.33	4.39	4.97	5.31
Pomfret	4.71	5.50	7.19	7.88	10.75	11.04
Escolar	2.41	2.81	3.06	3.08	3.22	3.90

Table S6: Complementary Analysis with Non-Eddy Baseline: Hurdle model selection results for each of the 14 pelagic predators, including the configuration, the difference in AIC relative to the model with the lowest score (dAIC), and AIC weight (AICw). Model configuration is specified as Eq. # for Presence/Absence component|Eq. # for Positive Count component. For example, 2|1 indicates the gyre-wide configuration (Eq. 2) was used for the presence-absence component and the base model configuration (Eq. 1) was used for the positive count component. The null models included for comparison exclude all fixed and random effects.

		Presence/Absence			**Positive Count**					
Predator	**Config**	**Base**	**Gyre**	**Subregion**	**Base**	**Gyre**	**Subregion**	**dAIC**	**AICw**	**Selected**
Albacore	Null							54277.6	0	
	1|1	x			x			1312.6	0	
	2|1		x		x			785.4	0	
	1|2	x				x		1084.5	0	
	2|2		x			x		557.3	0	
	1|3	x					x	962.4	0	
	2|3		x				x	435.2	0	
	3|1			x	x			350.2	0	
	3|2			x		x		122.1	0	
	3|3			x			x	0	1	*
Bigeye Tuna	Null							33977.1	0	
	1|1	x			x			3853.3	0	
	2|1		x		x			3768.6	0	
	1|2	x				x		3767.5	0	
	2|2		x			x		3682.8	0	
	1|3	x					x	1819.6	0	
	2|3		x				x	1735.0	0	
	3|1			x	x			2033.7	0	
	3|2			x		x		1947.9	0	
	3|3			x			x	0	1	*

continued

		Presence/Absence			Positive Count					
Predator	**Config**	**Base**	**Gyre**	**Subregion**	**Base**	**Gyre**	**Subregion**	**dAIC**	**AICw**	**Selected**
Yellowfin Tuna	Null							39270.7	0	
	1|1	x			x			124.1	0	
	2|1		x		x			27.7	0	
	1|2	x				x		117.7	0	
	2|2		x			x		21.3	0	
	1|3	x					x	117.4	0	
	2|3		x				x	20.9	0	
	3|1			x	x			6.7	0.02	
	3|2			x		x		0.3	0.45	*
	3|3			x			x	0	0.53	
Skipjack Tuna	Null							31204.2	0	
	1|1	x			x			155.8	0	
	2|1		x		x			66.9	0	
	1|2	x				x		137.7	0	
	2|2		x			x		48.8	0	
	1|3	x					x	103.6	0	
	2|3		x				x	14.7	0	
	3|1			x	x			52.2	0	
	3|2			x		x		34.1	0	
	3|3			x			x	0	1	*

continued

		Presence/Absence			Positive Count					
Predator	**Config**	**Base**	**Gyre**	**Subregion**	**Base**	**Gyre**	**Subregion**	**dAIC**	**AICw**	**Selected**
Striped Marlin	Null							32822.2	0	
	1|1	x			x			1852.8	0	
	2|1		x		x			1785.1	0	
	1|2	x				x		1833.0	0	
	2|2		x			x		1765.3	0	
	1|3	x					x	989.3	0	
	2|3		x				x	921.6	0	
	3|1			x	x			863.5	0	
	3|2			x		x		843.7	0	
	3|3			x			x	0	1	*
Blue Marlin	Null							20206.6	0	
	1|1	x			x			441.2	0	
	2|1		x		x			373.6	0	
	1|2	x				x		414.9	0	
	2|2		x			x		347.3	0	
	1|3	x					x	412.6	0	
	2|3		x				x	345.0	0	
	3|1			x	x			28.6	0	
	3|2			x		x		2.3	0.24	*
	3|3			x			x	0	0.76	

continued

		Presence/Absence			Positive Count					
Predator	**Config**	**Base**	**Gyre**	**Subregion**	**Base**	**Gyre**	**Subregion**	**dAIC**	**AICw**	**Selected**
Shortbill Spearfish	Null							25760.8	0	
	1|1	x			x			628.1	0	
	2|1		x		x			472.3	0	
	1|2	x				x		567.3	0	
	2|2		x			x		411.5	0	
	1|3	x					x	356.8	0	
	2|3		x				x	201.0	0	
	3|1			x	x			271.3	0	
	3|2			x		x		210.5	0	
	3|3			x			x	0	1	*
Swordfish	Null							11416.7	0	
	1|1	x			x			26.2	0	
	2|1		x		x			10.9	0	
	1|2	x				x		23.0	0	
	2|2		x			x		7.7	0.01	
	1|3	x					x	22.0	0	
	2|3		x				x	6.7	0.02	
	3|1			x	x			4.2	0.07	
	3|2			x		x		1.0	0.34	*
	3|3			x			x	0	0.56	

continued

		Presence/Absence			Positive Count					
Predator	**Config**	**Base**	**Gyre**	**Subregion**	**Base**	**Gyre**	**Subregion**	**dAIC**	**AICw**	**Selected**
Blue Shark	Null							56770.1	0	
	1|1	x			x			34.6	0	
	2|1		x		x			36.0	0	
	1|2	x				x		23.1	0	
	2|2		x			x		24.5	0	
	1|3	x					x	0.5	0.36	*
	2|3		x				x	2.0	0.17	
	3|1			x	x			34.0	0	
	3|2			x		x		22.5	0	
	3|3			x			x	0	0.47	
Wahoo	Null							42824.7	0	
	1|1	x			x			2514.8	0	
	2|1		x		x			2375.7	0	
	1|2	x				x		2466.7	0	
	2|2		x			x		2327.5	0	
	1|3	x					x	2000.3	0	
	2|3		x				x	1861.1	0	
	3|1			x	x			514.5	0	
	3|2			x		x		466.4	0	
	3|3			x			x	0	1	*

continued

		Presence/Absence			Positive Count					
Predator	**Config**	**Base**	**Gyre**	**Subregion**	**Base**	**Gyre**	**Subregion**	**dAIC**	**AICw**	**Selected**
Dolphinfish	Null							56222.8	0	
	1|1	x			x			455.5	0	
	2|1		x		x			430.2	0	
	1|2	x				x		446.3	0	
	2|2		x			x		421.0	0	
	1|3	x					x	25.3	0	
	2|3		x				x	0	0.78	*
	3|1			x	x			432.8	0	
	3|2			x		x		423.6	0	
	3|3			x			x	2.6	0.22	
Opah	Null							42542.4	0	
	1|1	x			x			351.8	0	
	2|1		x		x			331.8	0	
	1|2	x				x		351.7	0	
	2|2		x			x		331.7	0	
	1|3	x					x	299.4	0	
	2|3		x				x	279.4	0	
	3|1			x	x			52.4	0	
	3|2			x		x		52.4	0	
	3|3			x			x	0	1	*

continued

		Presence/Absence			Positive Count					
Predator	**Config**	**Base**	**Gyre**	**Subregion**	**Base**	**Gyre**	**Subregion**	**dAIC**	**AICw**	**Selected**
Pomfret	Null							42860.9	0	
	1|1	x			x			9258.9	0	
	2|1		x		x			9079.3	0	
	1|2	x				x		8824.0	0	
	2|2		x			x		8644.5	0	
	1|3	x					x	2664.5	0	
	2|3		x				x	2485.0	0	
	3|1			x	x			6594.4	0	
	3|2			x		x		6159.6	0	
	3|3			x			x	0	1	*
Escolar	Null							51689.8	0	
	1|1	x			x			492.0	0	
	2|1		x		x			298.1	0	
	1|2	x				x		205.1	0	
	2|2		x			x		11.2	0	
	1|3	x					x	193.9	0	
	2|3		x				x	0	0.55	*
	3|1			x	x			298.6	0	
	3|2			x		x		11.6	0	
	3|3			x			x	0.4	0.44	

Table S7: Complementary Analysis with Non-Eddy Baseline: Summary of model-estimated catch odds and rate ratios across species. Results are shown within each EKE subregion and across them.

EKE	Ratio	Comparison	Min	1st Qu.	Median	Mean	3rd Qu.	Max	N
High	Odds	Cyclone/Non-Eddy	0.80	0.92	0.96	0.95	0.98	1.07	14
		Anticyclone/Non-Eddy	0.88	1.02	1.08	1.07	1.13	1.29	14
		Anticyclone/Cyclone	0.90	1.07	1.15	1.13	1.19	1.39	14
	Rate	Cyclone/Non-Eddy	0.90	0.92	0.97	0.97	1.01	1.06	14
		Anticyclone/Non-Eddy	0.96	0.99	1.06	1.06	1.11	1.23	14
		Anticyclone/Cyclone	0.94	1.05	1.08	1.10	1.19	1.25	14
Low	Odds	Cyclone/Non-Eddy	0.74	0.87	0.94	0.93	0.99	1.07	14
		Anticyclone/Non-Eddy	0.99	1.02	1.05	1.06	1.07	1.23	14
		Anticyclone/Cyclone	0.97	1.06	1.13	1.16	1.21	1.66	14
	Rate	Cyclone/Non-Eddy	0.83	0.91	0.94	0.94	0.97	1.03	14
		Anticyclone/Non-Eddy	0.98	1.00	1.02	1.05	1.07	1.28	14
		Anticyclone/Cyclone	0.99	1.05	1.08	1.13	1.18	1.54	14
Both	Odds	Cyclone/Non-Eddy	0.74	0.90	0.95	0.94	0.98	1.07	28
		Anticyclone/Non-Eddy	0.88	1.02	1.06	1.07	1.11	1.29	28
		Anticyclone/Cyclone	0.90	1.06	1.14	1.15	1.21	1.66	28
	Rate	Cyclone/Non-Eddy	0.83	0.91	0.96	0.95	1.00	1.06	28
		Anticyclone/Non-Eddy	0.96	0.99	1.03	1.05	1.10	1.28	28
		Anticyclone/Cyclone	0.94	1.05	1.08	1.11	1.19	1.54	28

Table S8: Summary of eddy characteristics across the study region based on daily eddy realizations (visualized in Fig. S21).

Characteristic	EKE	Polarity	Min	1st Qu.	Median	Mean	3rd Qu.	Max	N
Amplitude (cm)	High	Anticyclone	1.0	4.1	6.5	7.3	9.7	29.8	217,090
		Cyclone	1.0	4.0	6.3	7.3	9.5	47.0	226,320
	Low	Anticyclone	1.0	2.6	3.9	4.7	6.0	23.5	330,370
		Cyclone	1.0	2.7	4.3	5.1	6.5	30.2	354,030
Radius (km)	High	Anticyclone	14.6	72.7	94.4	100.5	122.4	336.4	217,090
		Cyclone	14.6	69.3	90.2	97.6	119.5	329.1	226,320
	Low	Anticyclone	14.6	69.5	90.3	99.0	118.6	357.9	330,370
		Cyclone	14.6	68.6	87.6	95.3	114.1	337.3	354,030
Rotational Velocity (m/s)	High	Anticyclone	4.3	15.8	20.0	20.9	25.2	56.1	217,090
		Cyclone	4.9	15.7	20.1	21.2	25.4	99.5	226,320
	Low	Anticyclone	3.4	10.8	13.8	14.5	17.5	49.5	330,370
		Cyclone	3.4	11.0	14.7	15.9	19.5	64.8	354,030
Age (days)	High	Anticyclone	1	30	77	129	174	1463	217,090
		Cyclone	1	30	74	124	170	1412	226,320
	Low	Anticyclone	1	25	60	112	142	1442	330,370
		Cyclone	1	25	59	102	137	903	354,030

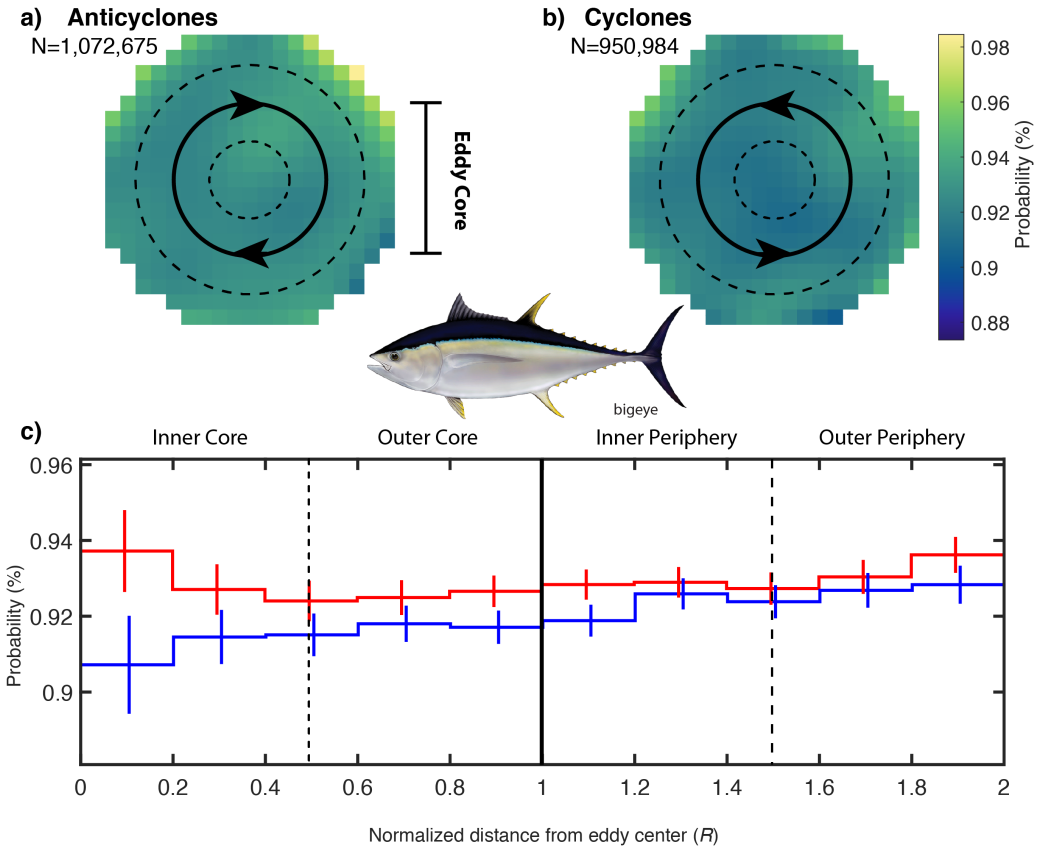

Figure S1: Example eddy-centric 2D (a, b) and 1D (c) composites of bigeye tuna catch probability – the % of longline sets catching at least one bigeye tuna – from the nominal fishery data across the study region. In panels a–c, the eddy core ($0 - R$) and periphery ($R - 2R$) are separated by the solid black line, and the inner and outer zones of both the core ($0 - 0.5R$ & $0.5R - R$) and periphery ($R - 1.5R$ & $1.5R - 2R$) are separated by the dashed black lines. In panels a and b, N represents the total number of individuals captured in eddies of the respective polarities, catch probability is calculated per $0.2R$ x $0.2R$ cell, and north is up. In panel c, N per polarity is the same as in panels a and b, anticyclonic values are red and cyclonic values are blue, and polarity-specific mean catch probability (with the 95% confidence interval) is calculated per $0.2R$ width bin.

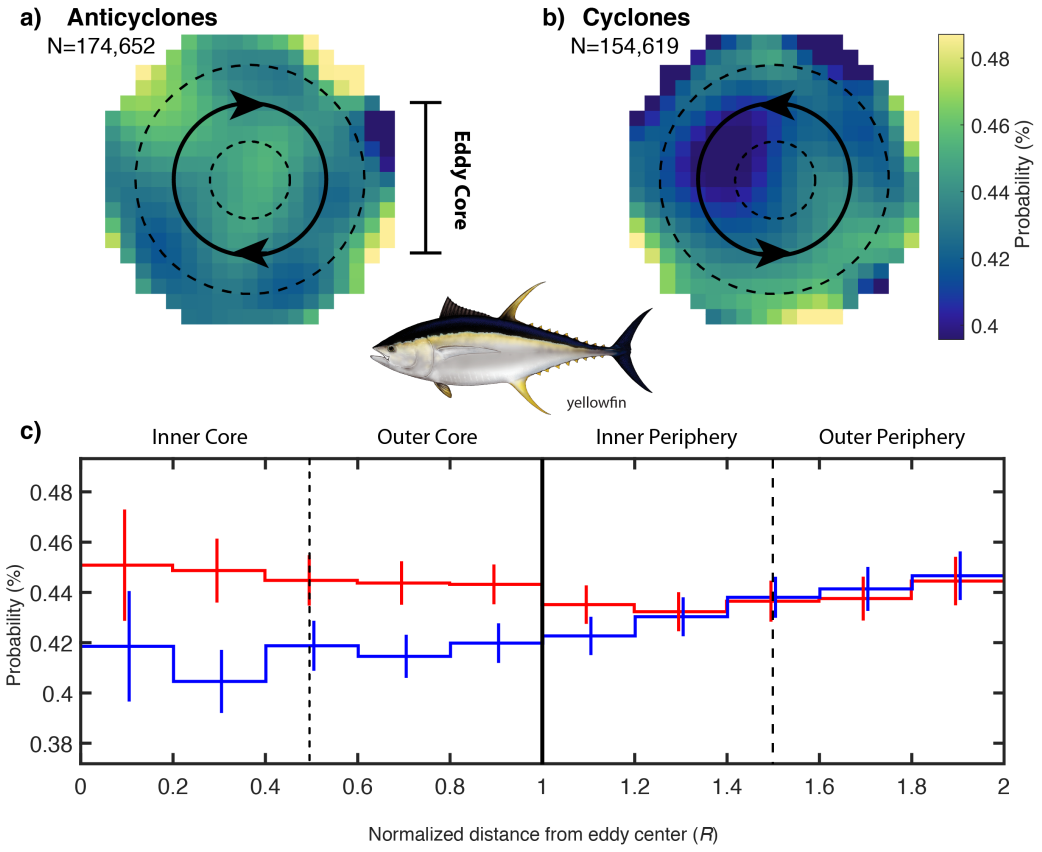

Figure S2: Example eddy-centric 2D (a, b) and 1D (c) composites of yellowfin tuna catch probability – the % of longline sets catching at least one yellowfin tuna – from the nominal fishery data across the study region. In panels a–c, the eddy core ($0 - R$) and periphery ($R - 2R$) are separated by the solid black line, and the inner and outer zones of both the core ($0 - 0.5R$ & $0.5R - R$) and periphery ($R - 1.5R$ & $1.5R - 2R$) are separated by the dashed black lines. In panels a and b, N represents the total number of individuals captured in eddies of the respective polarities, catch probability is calculated per $0.2R$ x $0.2R$ cell, and north is up. In panel c, N per polarity is the same as in panels a and b, anticyclonic values are red and cyclonic values are blue, and polarity-specific mean catch probability (with the 95% confidence interval) is calculated per $0.2R$ width bin.

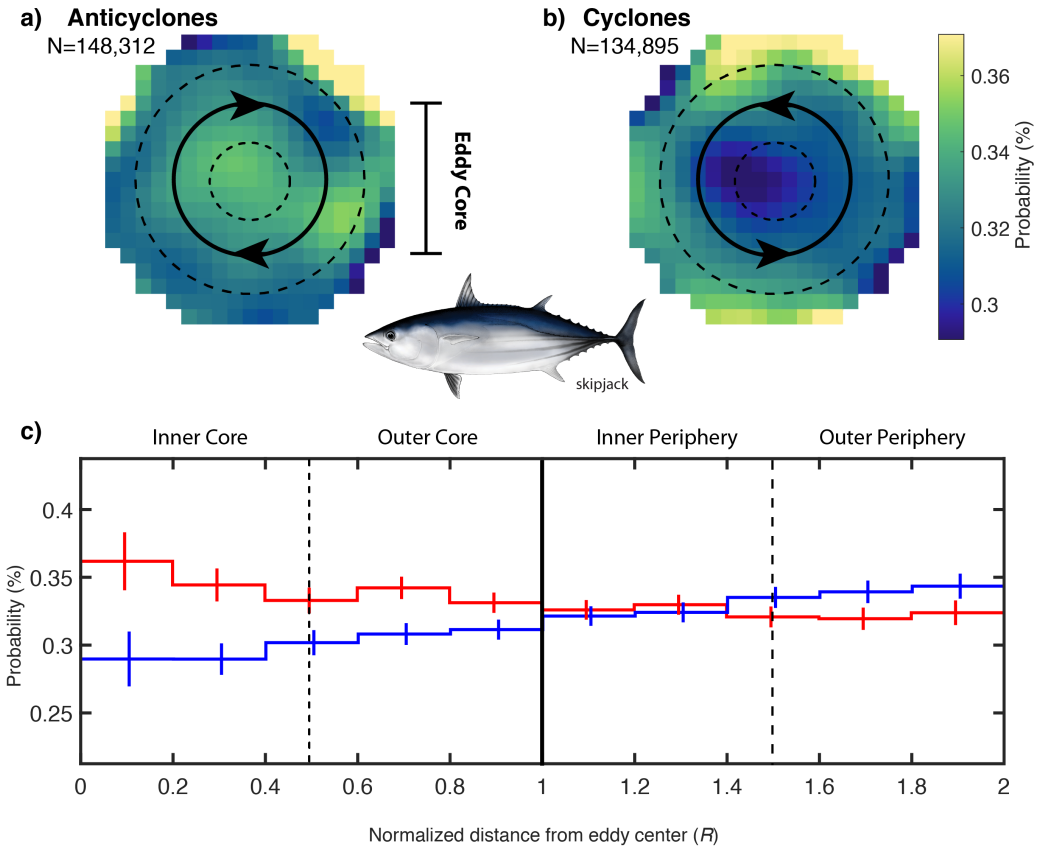

Figure S3: Nominal eddy-centric skipjack tuna catch: Example eddy-centric 2D (a, b) and 1D (c) composites of skipjack tuna catch probability – the % of longline sets catching at least one skipjack tuna – from the nominal fishery data across the study region. In panels a–c, the eddy core (0 – R) and periphery (R – $2R$) are separated by the solid black line, and the inner and outer zones of both the core (0 – $0.5R$ & $0.5R$ – R) and periphery (R – $1.5R$ & $1.5R$ – $2R$) are separated by the dashed black lines. In panels a and b, N represents the total number of individuals captured in eddies of the respective polarities, catch probability is calculated per $0.2R$ x $0.2R$ cell, and north is up. In panel c, N per polarity is the same as in panels a and b, anticyclonic values are red and cyclonic values are blue, and polarity-specific mean catch probability (with the 95% confidence interval) is calculated per $0.2R$ width bin.

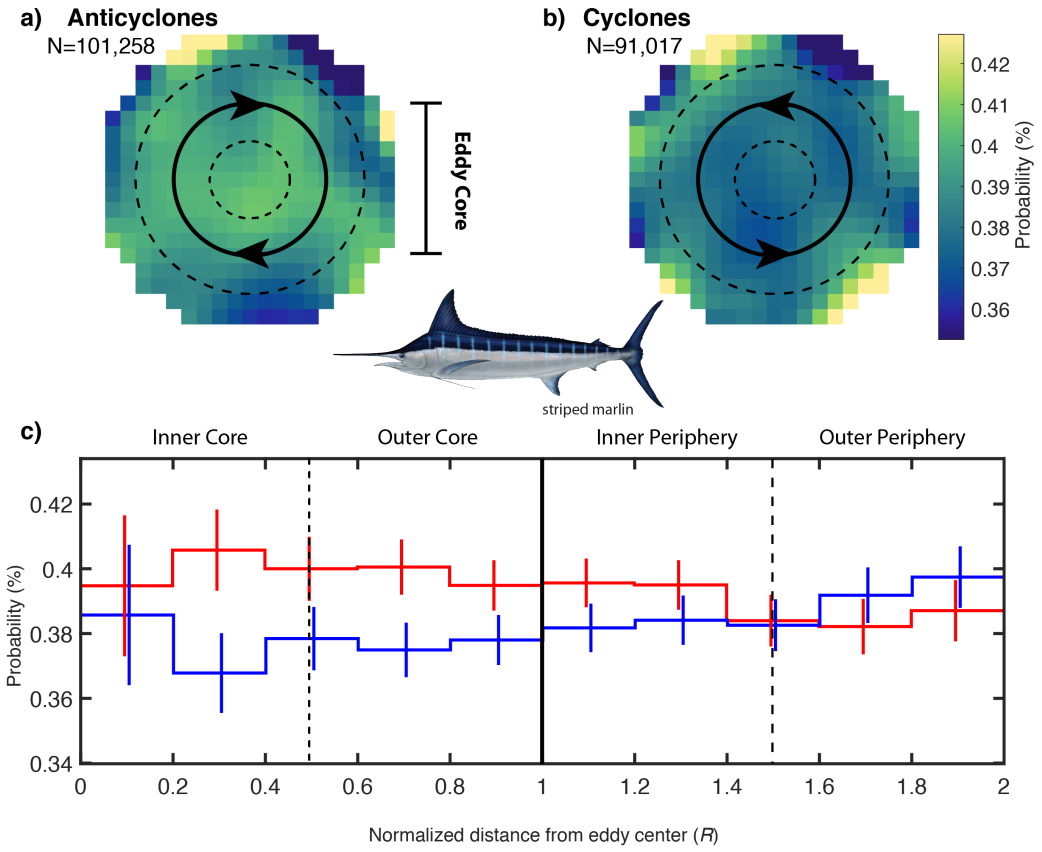

Figure S4: Nominal eddy-centric striped marlin catch: Example eddy-centric 2D (a, b) and 1D (c) composites of striped marlin catch probability – the % of longline sets catching at least one striped marlin – from the nominal fishery data across the study region. In panels a–c, the eddy core ($0 - R$) and periphery ($R - 2R$) are separated by the solid black line, and the inner and outer zones of both the core ($0 - 0.5R$ & $0.5R - R$) and periphery ($R - 1.5R$ & $1.5R - 2R$) are separated by the dashed black lines. In panels a and b, N represents the total number of individuals captured in eddies of the respective polarities, catch probability is calculated per $0.2R$ x $0.2R$ cell, and north is up. In panel c, N per polarity is the same as in panels a and b, anticyclonic values are red and cyclonic values are blue, and polarity-specific mean catch probability (with the 95% confidence interval) is calculated per $0.2R$ width bin.

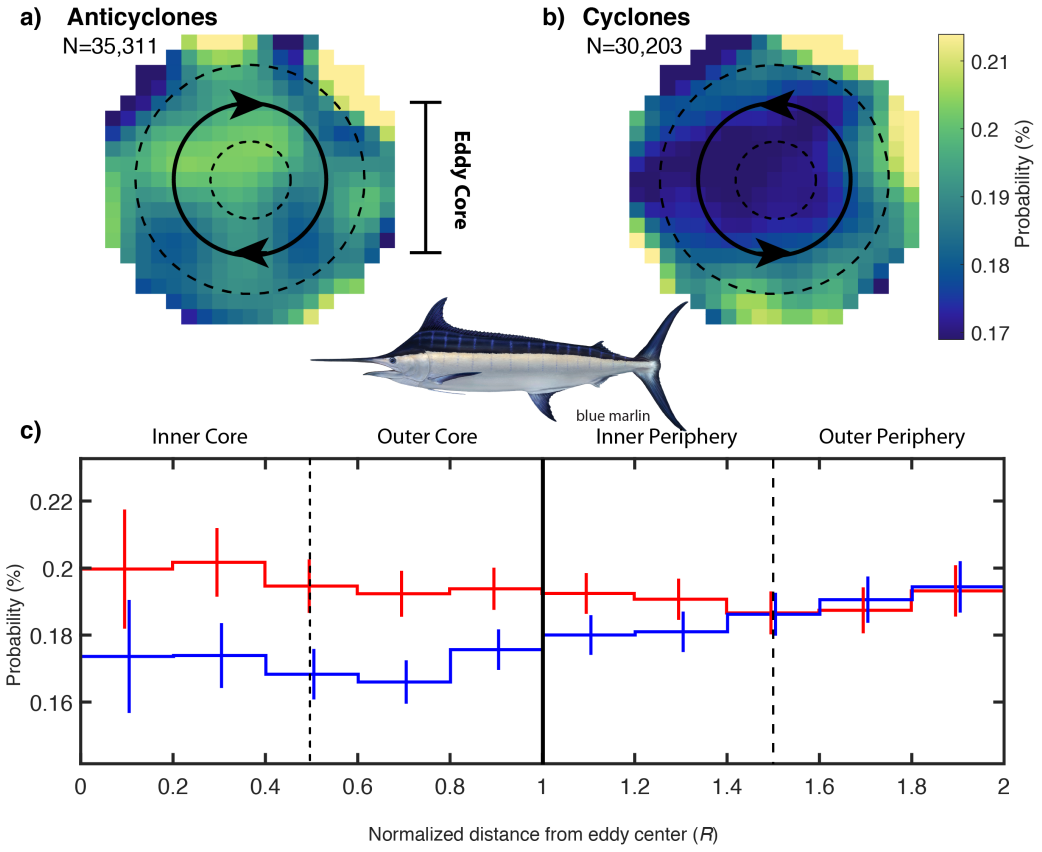

Figure S5: Nominal eddy-centric blue marlin catch: Example eddy-centric 2D (a, b) and 1D (c) composites of blue marlin catch probability – the % of longline sets catching at least one blue marlin – from the nominal fishery data across the study region. In panels a–c, the eddy core ($0 - R$) and periphery ($R - 2R$) are separated by the solid black line, and the inner and outer zones of both the core ($0 - 0.5R$ & $0.5R - R$) and periphery ($R - 1.5R$ & $1.5R - 2R$) are separated by the dashed black lines. In panels a and b, N represents the total number of individuals captured in eddies of the respective polarities, catch probability is calculated per $0.2R$ x $0.2R$ cell, and north is up. In panel c, N per polarity is the same as in panels a and b, anticyclonic values are red and cyclonic values are blue, and polarity-specific mean catch probability (with the 95% confidence interval) is calculated per $0.2R$ width bin.

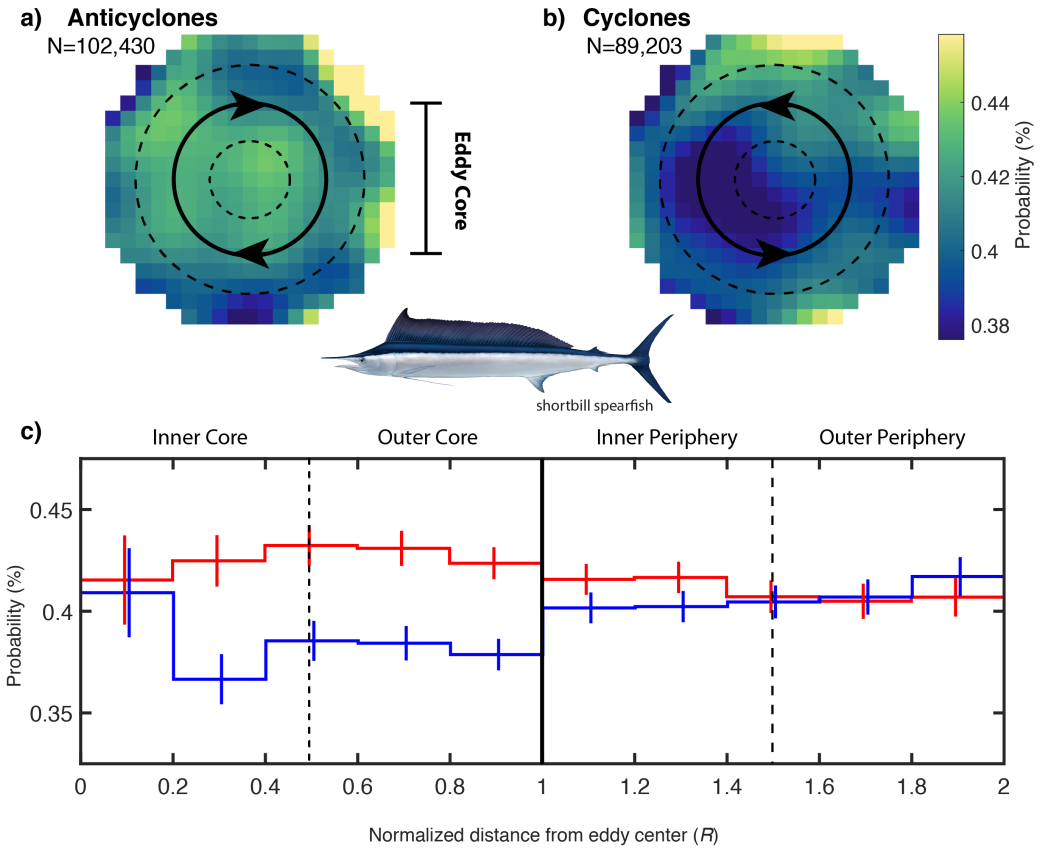

Figure S6: Nominal eddy-centric shortbill spearfish catch: Example eddy-centric 2D (a, b) and 1D (c) composites of shortbill spearfish catch probability – the % of longline sets catching at least one shortbill spearfish – from the nominal fishery data across the study region. In panels a–c, the eddy core (0 – R) and periphery (R – $2R$) are separated by the solid black line, and the inner and outer zones of both the core (0 – $0.5R$ & $0.5R$ – R) and periphery (R – $1.5R$ & $1.5R$ – $2R$) are separated by the dashed black lines. In panels a and b, N represents the total number of individuals captured in eddies of the respective polarities, catch probability is calculated per $0.2R$ x $0.2R$ cell, and north is up. In panel c, N per polarity is the same as in panels a and b, anticyclonic values are red and cyclonic values are blue, and polarity-specific mean catch probability (with the 95% confidence interval) is calculated per $0.2R$ width bin.

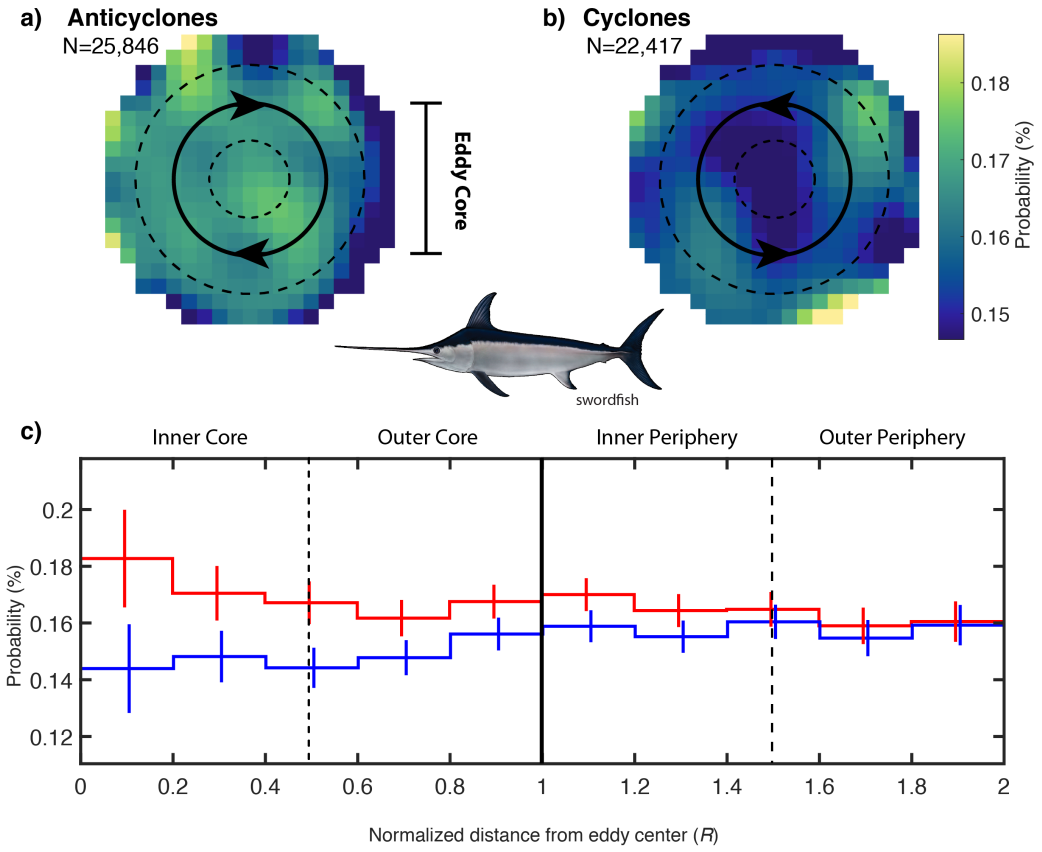

Figure S7: Nominal eddy-centric swordfish catch: Example eddy-centric 2D (a, b) and 1D (c) composites of swordfish catch probability – the % of longline sets catching at least one swordfish – from the nominal fishery data across the study region. In panels a–c, the eddy core (0 – R) and periphery (R – $2R$) are separated by the solid black line, and the inner and outer zones of both the core (0 – $0.5R$ & $0.5R$ – R) and periphery (R – $1.5R$ & $1.5R$ – $2R$) are separated by the dashed black lines. In panels a and b, N represents the total number of individuals captured in eddies of the respective polarities, catch probability is calculated per $0.2R$ x $0.2R$ cell, and north is up. In panel c, N per polarity is the same as in panels a and b, anticyclonic values are red and cyclonic values are blue, and polarity-specific mean catch probability (with the 95% confidence interval) is calculated per $0.2R$ width bin.

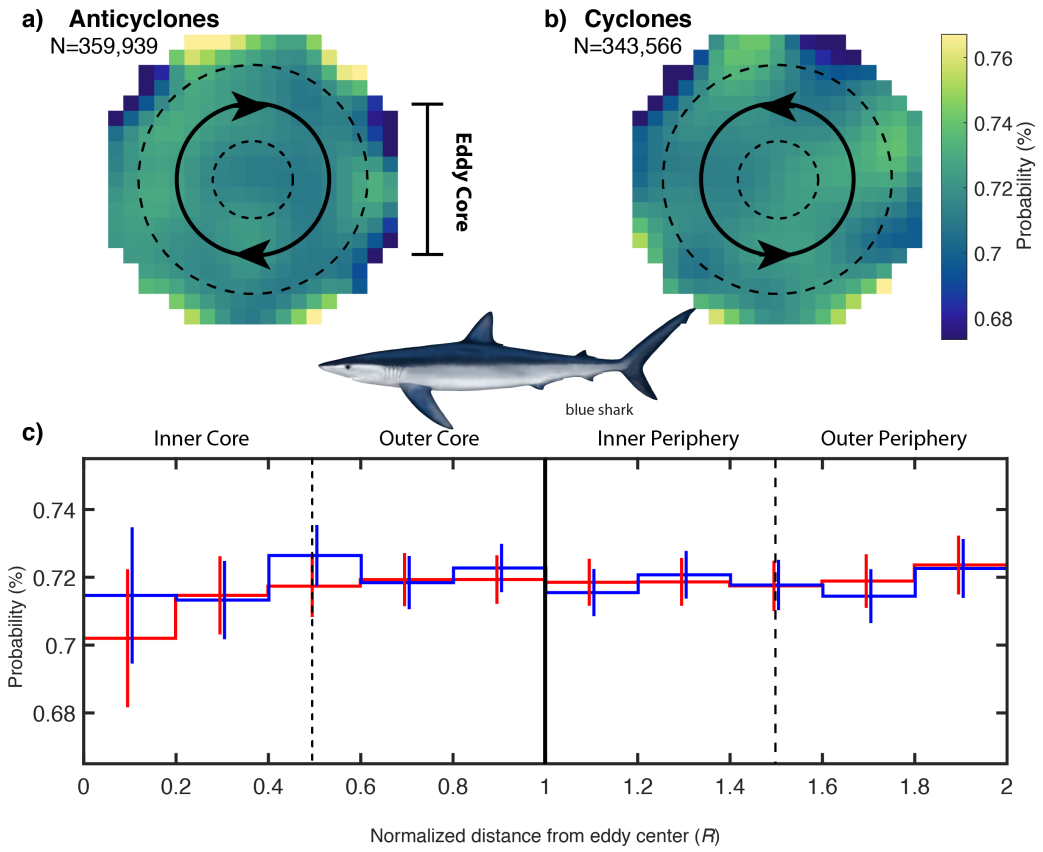

Figure S8: Nominal eddy-centric blue shark catch: Example eddy-centric 2D (a, b) and 1D (c) composites of blue shark catch probability – the % of longline sets catching at least one blue shark – from the nominal fishery data across the study region. In panels a–c, the eddy core (0 – R) and periphery (R – $2R$) are separated by the solid black line, and the inner and outer zones of both the core (0 – $0.5R$ & $0.5R$ – R) and periphery (R – $1.5R$ & $1.5R$ – $2R$) are separated by the dashed black lines. In panels a and b, N represents the total number of individuals captured in eddies of the respective polarities, catch probability is calculated per $0.2R$ x $0.2R$ cell, and north is up. In panel c, N per polarity is the same as in panels a and b, anticyclonic values are red and cyclonic values are blue, and polarity-specific mean catch probability (with the 95% confidence interval) is calculated per $0.2R$ width bin.

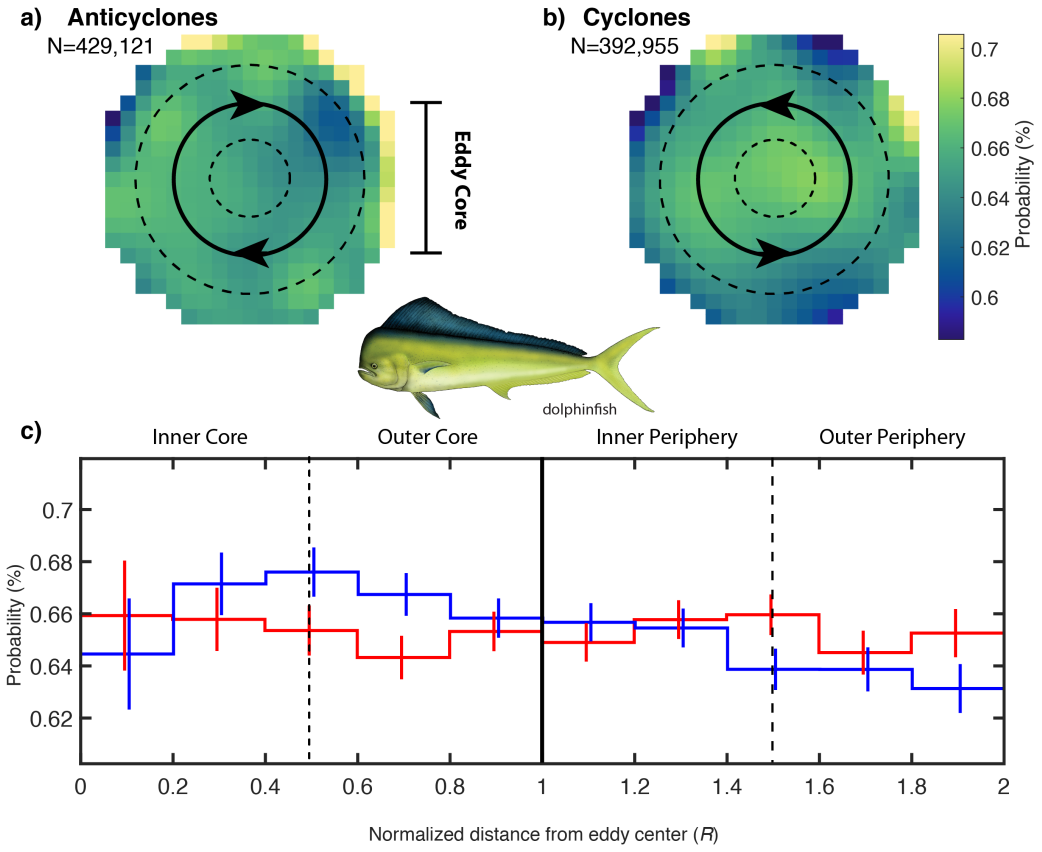

Figure S9: Nominal eddy-centric dolphinfish catch: Example eddy-centric 2D (a, b) and 1D (c) composites of dolphinfish catch probability – the % of longline sets catching at least one dolphinfish – from the nominal fishery data across the study region. In panels a–c, the eddy core (0 – R) and periphery (R – $2R$) are separated by the solid black line, and the inner and outer zones of both the core (0 – $0.5R$ & $0.5R$ – R) and periphery (R – $1.5R$ & $1.5R$ – $2R$) are separated by the dashed black lines. In panels a and b, N represents the total number of individuals captured in eddies of the respective polarities, catch probability is calculated per $0.2R$ x $0.2R$ cell, and north is up. In panel c, N per polarity is the same as in panels a and b, anticyclonic values are red and cyclonic values are blue, and polarity-specific mean catch probability (with the 95% confidence interval) is calculated per $0.2R$ width bin.

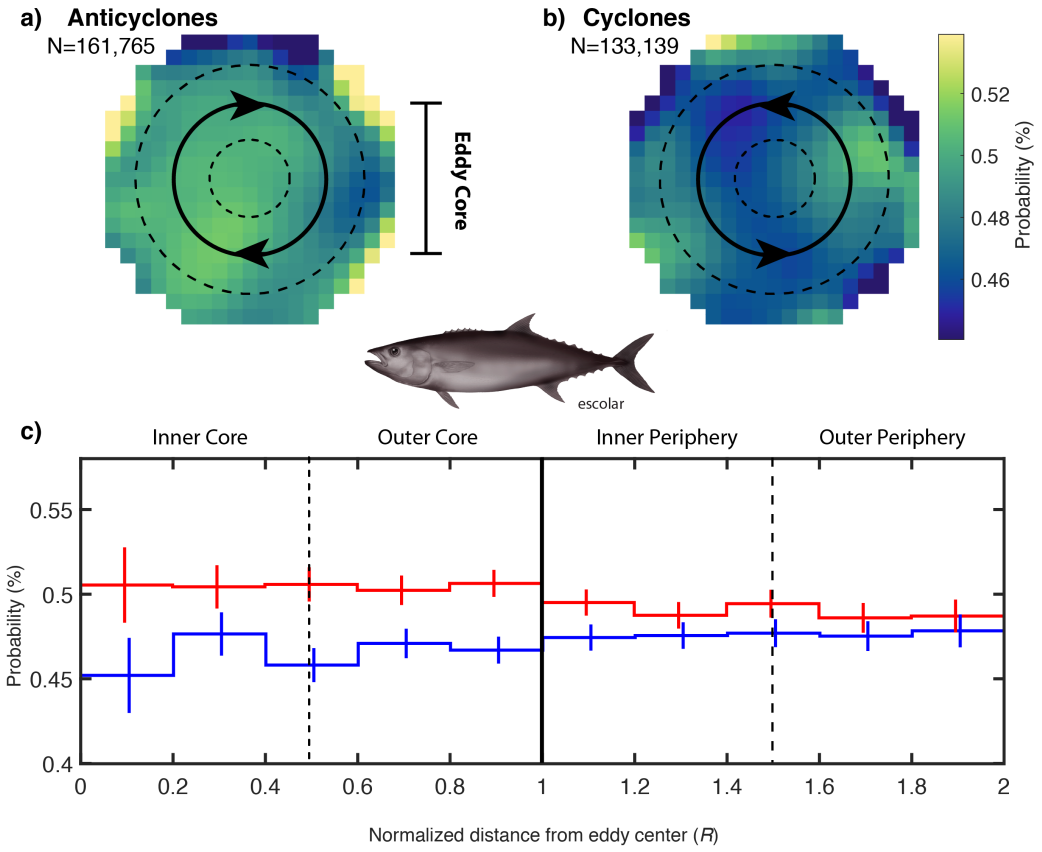

Figure S10: Nominal eddy-centric escolar catch: Example eddy-centric 2D (a, b) and 1D (c) composites of escolar catch probability – the % of longline sets catching at least one escolar – from the nominal fishery data across the study region. In panels a–c, the eddy core ($0 - R$) and periphery ($R - 2R$) are separated by the solid black line, and the inner and outer zones of both the core ($0 - 0.5R$ & $0.5R - R$) and periphery ($R - 1.5R$ & $1.5R - 2R$) are separated by the dashed black lines. In panels a and b, N represents the total number of individuals captured in eddies of the respective polarities, catch probability is calculated per $0.2R$ x $0.2R$ cell, and north is up. In panel c, N per polarity is the same as in panels a and b, anticyclonic values are red and cyclonic values are blue, and polarity-specific mean catch probability (with the 95% confidence interval) is calculated per $0.2R$ width bin.

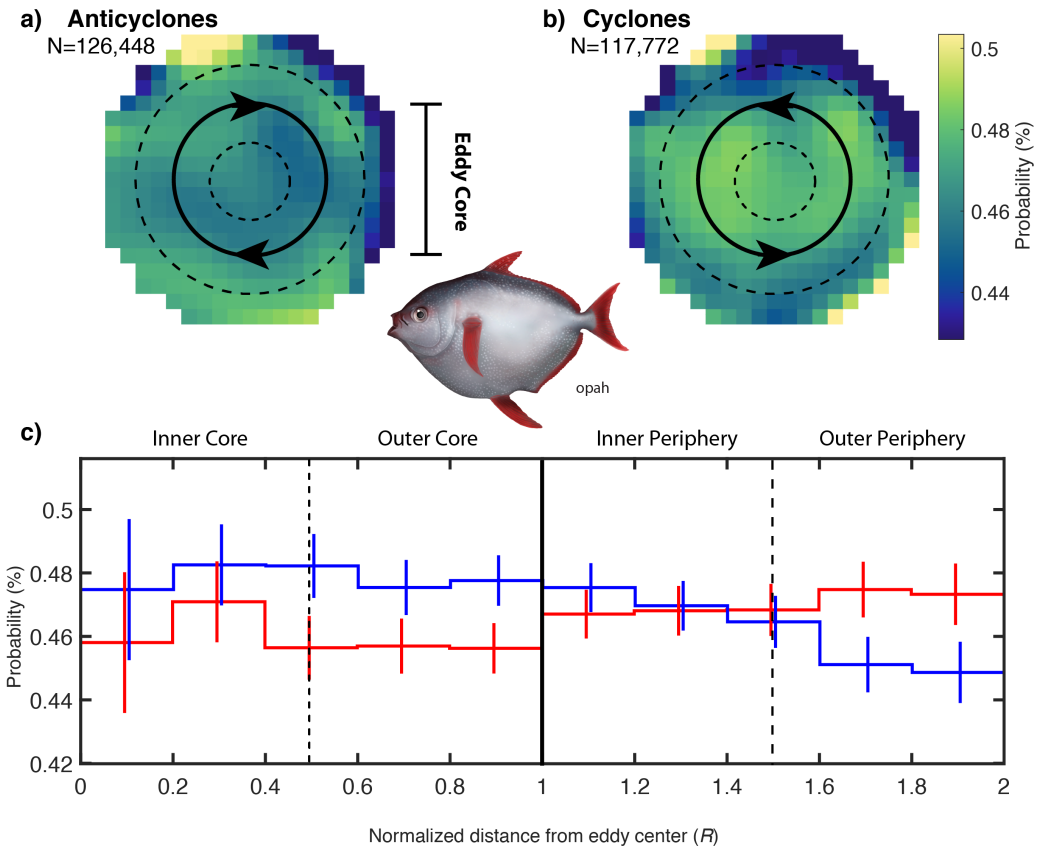

Figure S11: Nominal eddy-centric opah catch: Example eddy-centric 2D (a, b) and 1D (c) composites of opah catch probability – the % of longline sets catching at least one opah – from the nominal fishery data across the study region. In panels a–c, the eddy core ($0 - R$) and periphery ($R - 2R$) are separated by the solid black line, and the inner and outer zones of both the core ($0 - 0.5R$ & $0.5R - R$) and periphery ($R - 1.5R$ & $1.5R - 2R$) are separated by the dashed black lines. In panels a and b, N represents the total number of individuals captured in eddies of the respective polarities, catch probability is calculated per $0.2R$ x $0.2R$ cell, and north is up. In panel c, N per polarity is the same as in panels a and b, anticyclonic values are red and cyclonic values are blue, and polarity-specific mean catch probability (with the 95% confidence interval) is calculated per $0.2R$ width bin.

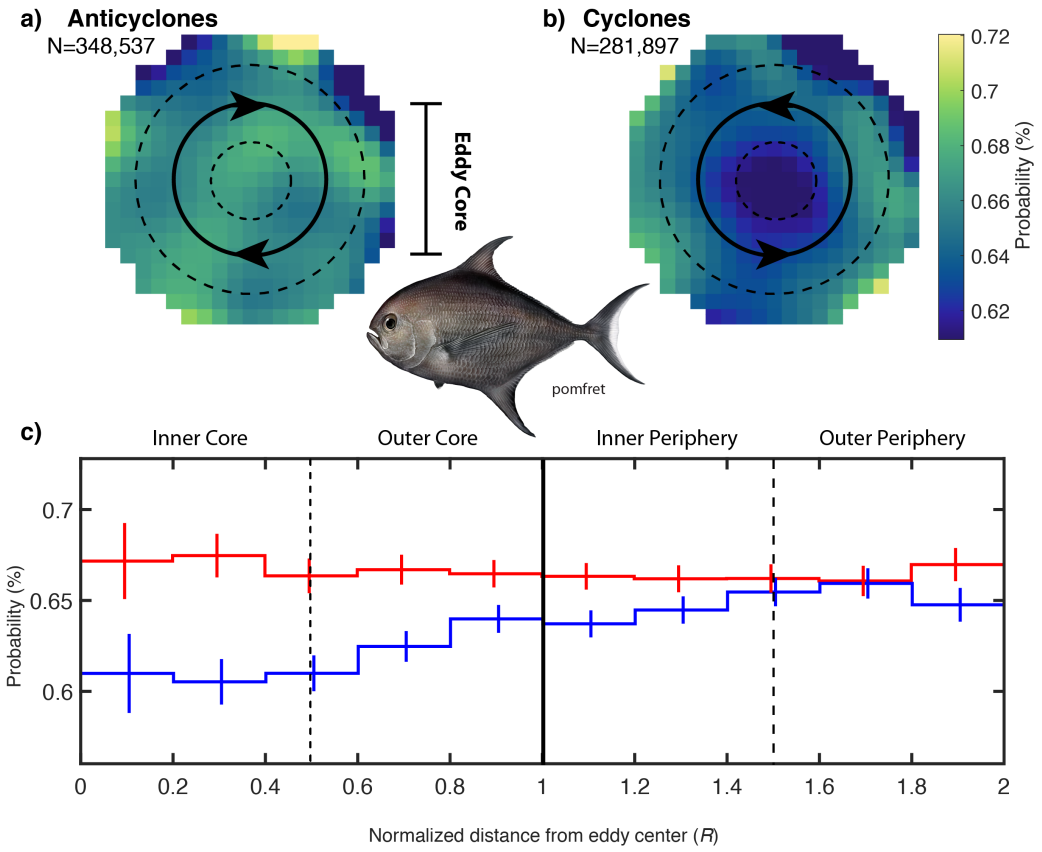

Figure S12: Nominal eddy-centric pomfret catch: Example eddy-centric 2D (a, b) and 1D (c) composites of pomfret catch probability – the % of longline sets catching at least one pomfret – from the nominal fishery data across the study region. In panels a–c, the eddy core (0 – R) and periphery (R – $2R$) are separated by the solid black line, and the inner and outer zones of both the core (0 – $0.5R$ & $0.5R$ – R) and periphery (R – $1.5R$ & $1.5R$ – $2R$) are separated by the dashed black lines. In panels a and b, N represents the total number of individuals captured in eddies of the respective polarities, catch probability is calculated per $0.2R$ x $0.2R$ cell, and north is up. In panel c, N per polarity is the same as in panels a and b, anticyclonic values are red and cyclonic values are blue, and polarity-specific mean catch probability (with the 95% confidence interval) is calculated per $0.2R$ width bin.

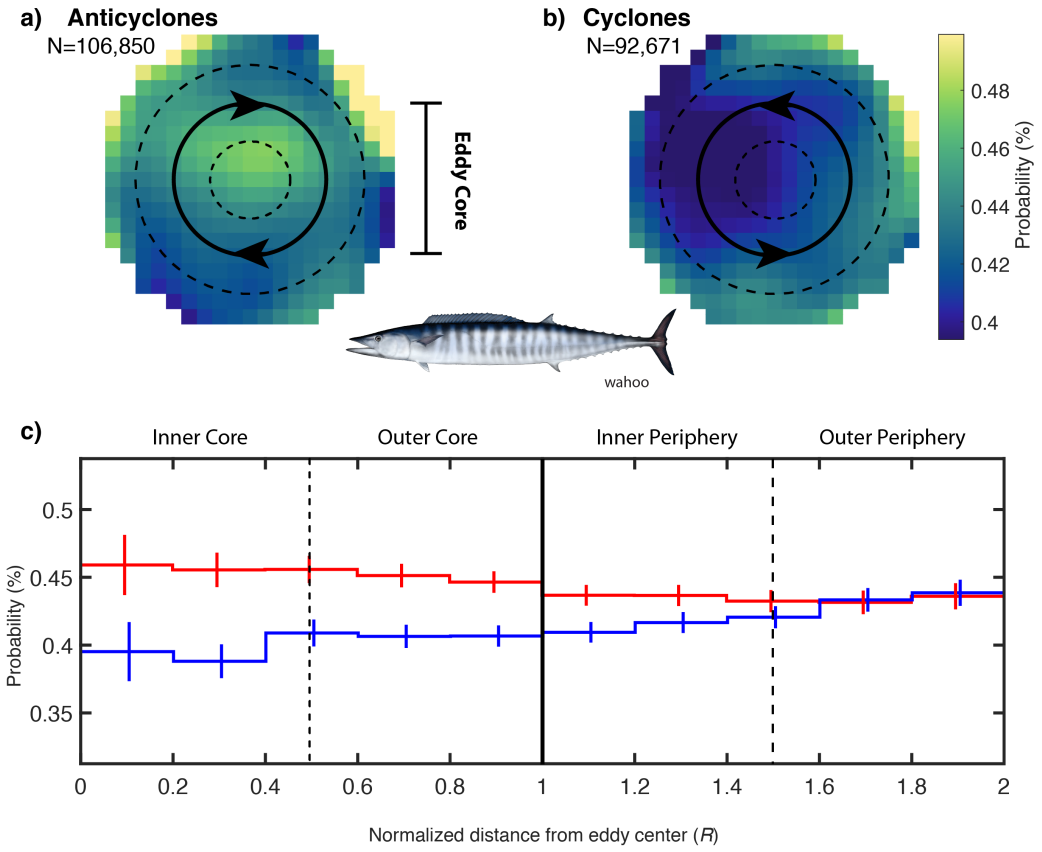

Figure S13: Nominal eddy-centric wahoo catch: Example eddy-centric 2D (a, b) and 1D (c) composites of wahoo catch probability – the % of longline sets catching at least one wahoo – from the nominal fishery data across the study region. In panels a–c, the eddy core ($0 - R$) and periphery ($R - 2R$) are separated by the solid black line, and the inner and outer zones of both the core ($0 - 0.5R$ & $0.5R - R$) and periphery ($R - 1.5R$ & $1.5R - 2R$) are separated by the dashed black lines. In panels a and b, N represents the total number of individuals captured in eddies of the respective polarities, catch probability is calculated per $0.2R$ x $0.2R$ cell, and north is up. In panel c, N per polarity is the same as in panels a and b, anticyclonic values are red and cyclonic values are blue, and polarity-specific mean catch probability (with the 95% confidence interval) is calculated per $0.2R$ width bin.

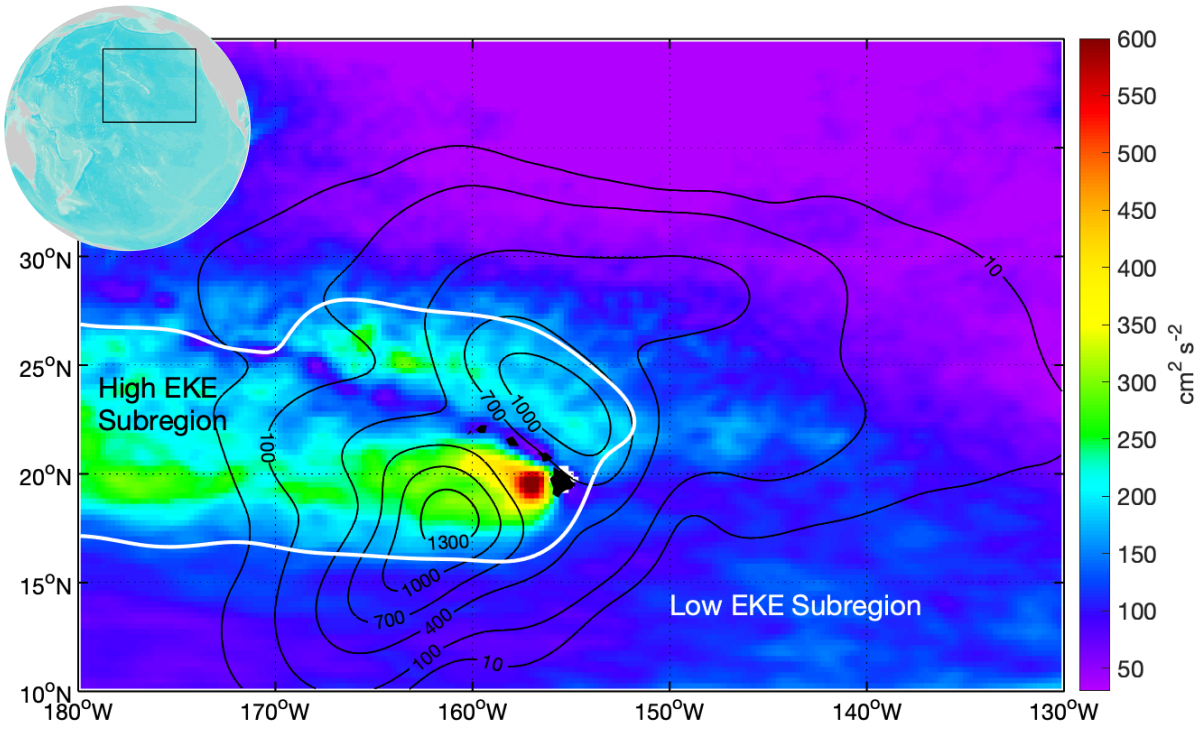

Figure S14: Eddy kinetic energy field: Mean eddy kinetic energy (EKE) derived from sea surface height. The eddy dynamics subregions are demarcated by the 150 $cm^2 s^{-2}$ contour (white) from a smoothed version of the data shown in the pseudocolor image. Fishing effort co-located to eddies is contoured (black) by the smoothed number of longline sets per degree^2; the division of effort among eddy dynamics subregions is nearly equal – low EKE, n = 112,105; high EKE, n = 107,929.

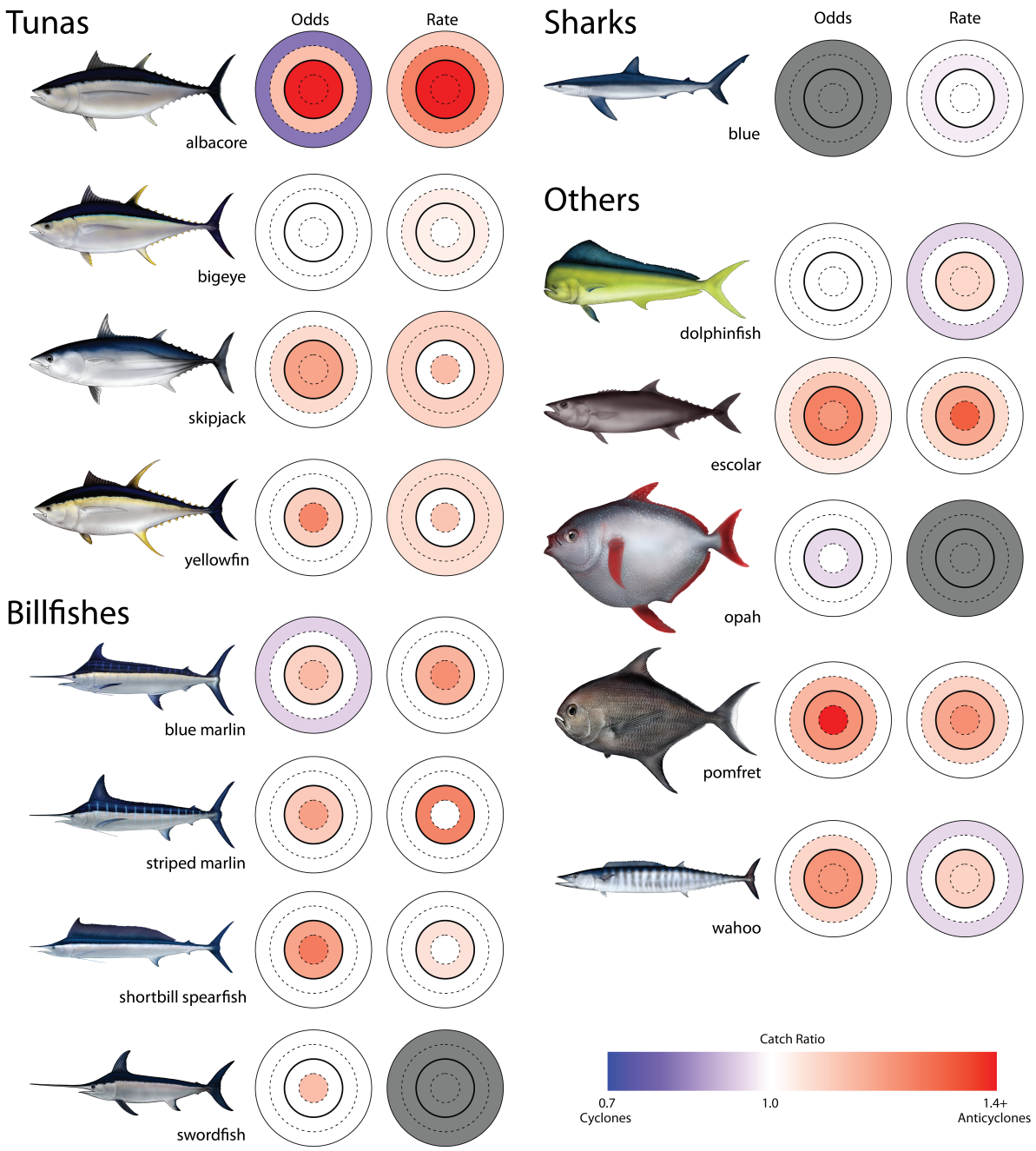

Figure S15: Eddy-centric catch metrics (low EKE): Catch odds ratios and catch rate ratios comparing a given zone of anticyclones against the corresponding zone of cyclones. Ratios of catch metrics are color coded; > 1 - significantly higher in anticyclones (red), < 1 - significantly higher in cyclones (blue), $= 1$ - not significantly different among polarities (white), N/A - best-fit model did not include eddy-related effects for that metric (grey). Ratio values > 1.4 were truncated to aid in color discernment. Ratios not significantly different among polarities were set to equal 1. Eddy cores are separated from peripheries by the solid black line, and both are further differentiated into inner and outer zones by the dashed black lines. These model-estimated ratios come from the low EKE subregion, but see Fig. 2 for the ratios from the high EKE subregion and Fig. S16 for the full results (ratios in both the high and low EKE subregions, including 95% confidence intervals determined with the delta method).

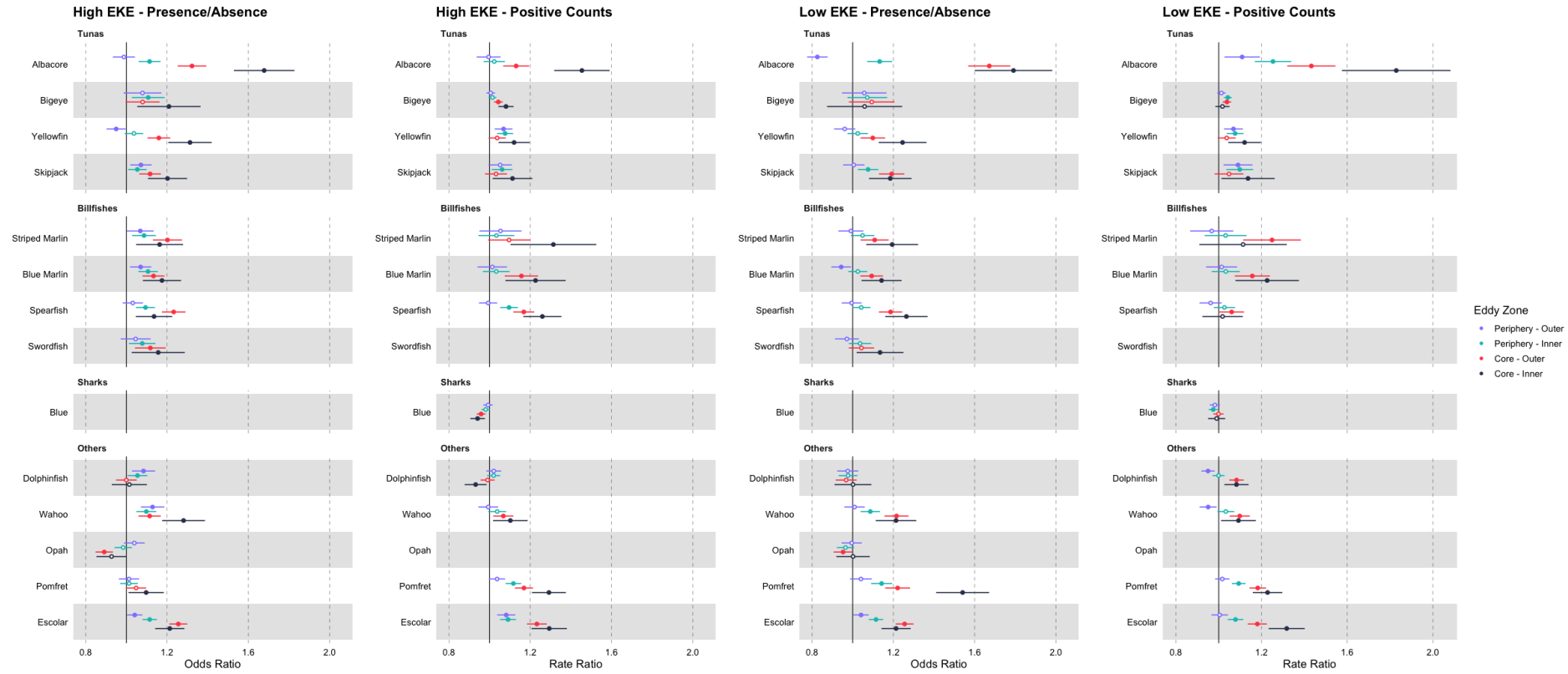

Figure S16: Eddy-Centric Analysis: Species-specific odds and rate ratios, separated by eddy dynamics subregion, comparing catch metrics in a given zone of an anticyclone against the corresponding zone of a cyclone. The mean effect estimate (circle) is filled when significant and open when not significant. The vertical black line indicates a ratio of 1 (equal odds or rates); if a 95% confidence interval (determined with the delta method) passes through this line the corresponding estimate is not significant. Missing estimates indicate that the best-fit model for that species did not include eddy-related effects in that component of the hurdle model. Identical estimates among the eddy dynamics subregions indicate that the best-fit model for that species included gyre-wide estimates in that component of the hurdle model. Each species-specific model used N = 220,034 longline sets (except that for blue shark, which used 219,837).

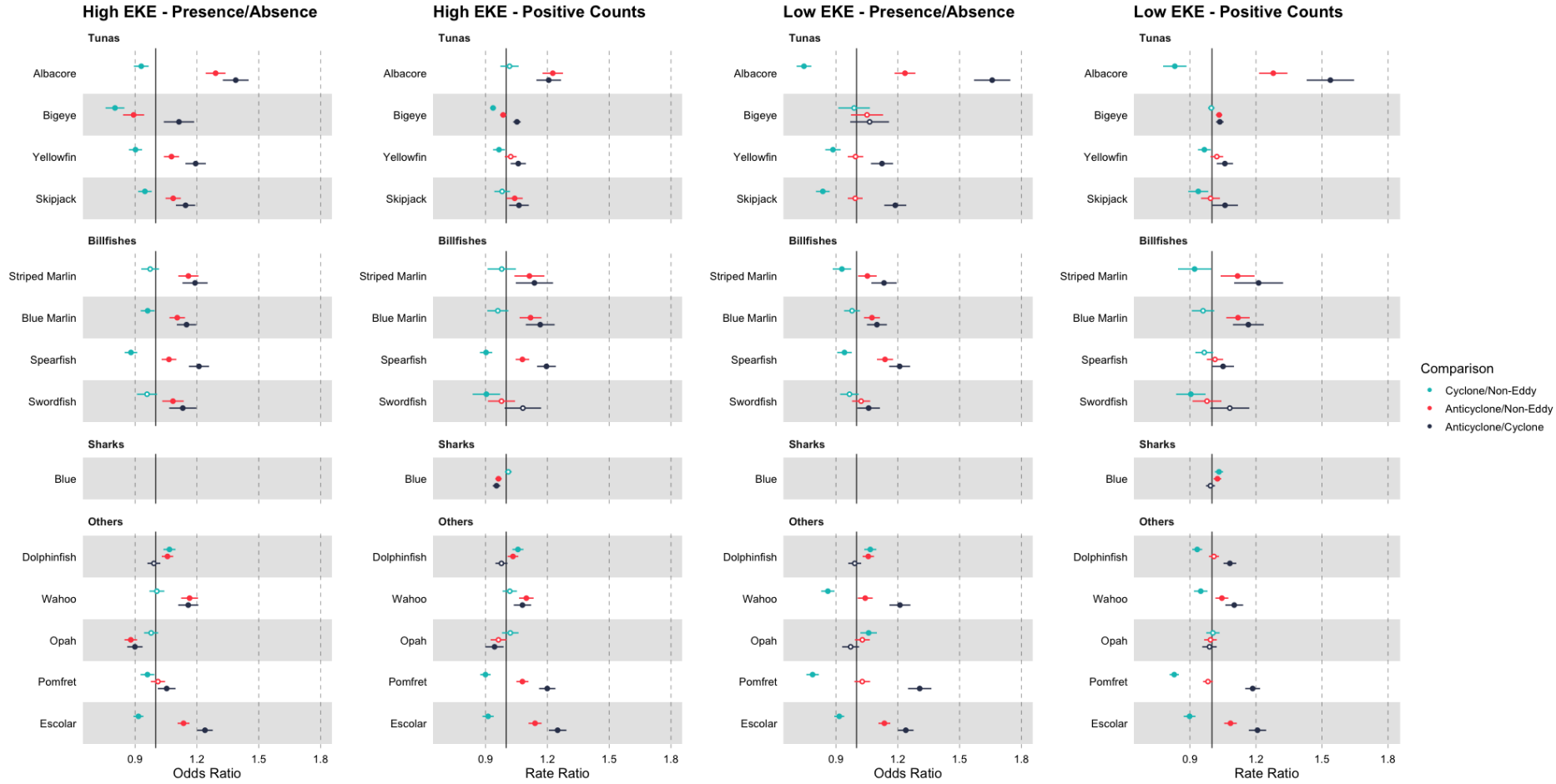

Figure S17: Complementary Analysis with Non-Eddy Baseline: Species-specific odds and rate ratios, separated by eddy dynamics subregion, comparing catch metrics among the cores of eddies of both polarities and non-eddy areas. The mean effect estimate (circle) is filled when significant and open when not significant. The vertical black line indicates a ratio of 1 (equal odds or rates); if a 95% confidence interval (determined with the delta method) passes through this line the corresponding estimate is not significant. Missing estimates indicate that the best-fit model for that species did not include eddy-related effects in that component of the hurdle model. Identical estimates among the eddy dynamics subregions indicate that the best-fit model for that species included gyre-wide estimates in that component of the hurdle model. Each species-specific model used N = 182,775 longline sets (except for blue shark, which used 182,629), and effect estimate significance was determined with the delta method.

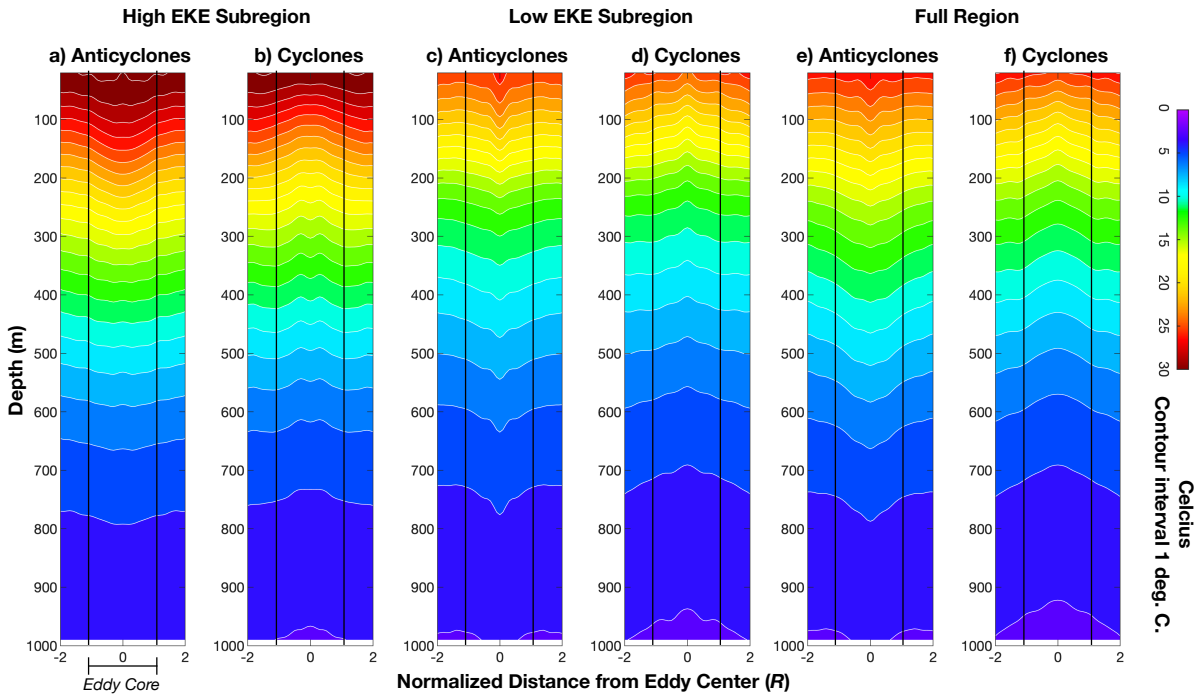

Figure S18: Eddy vertical thermal structure: Vertical temperature composites of anticyclones and cyclones within the high and low EKE subregions, as well as across the full study region. The vertical solid black lines at $|R| = 1$ designate the transition from the core (i.e., interior) to periphery (i.e., exterior) of an eddy. Sample size (number of Argo profiles) per panel – a) n = 6,808; b) n = 6,752; c) n = 19,362; d) n = 20,145, e) n = 26,170; f) n = 26,897.

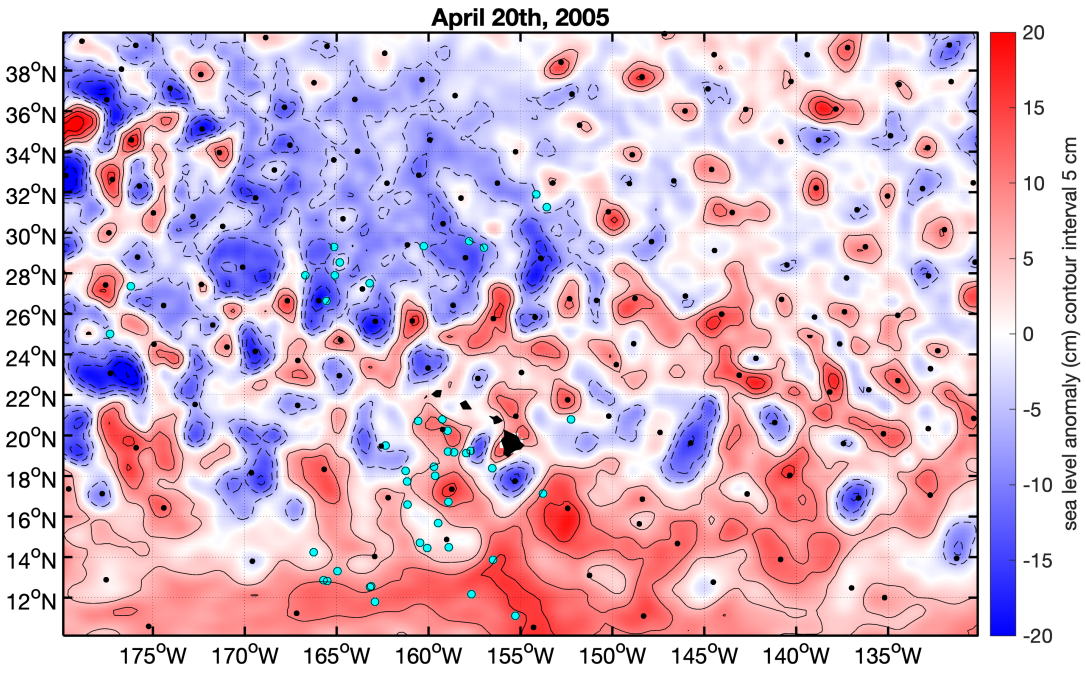

Figure S19: Example eddy co-location: Example of mock longline sets co-located to eddies from AVISO's Mesoscale Eddy Trajectory Atlas and the associated sea level anomaly (SLA) on a given day. Colored points denote locations of eddy centers (black) and mock longline sets (cyan). Positive SLA is associated with anticyclones and negative SLA with cyclones. Contours of SLA (positive - solid; negative - dashed) are provided at 5-cm internals. The longline set locations in this example were randomly generated and did not use real fishing locations due to privacy restrictions.

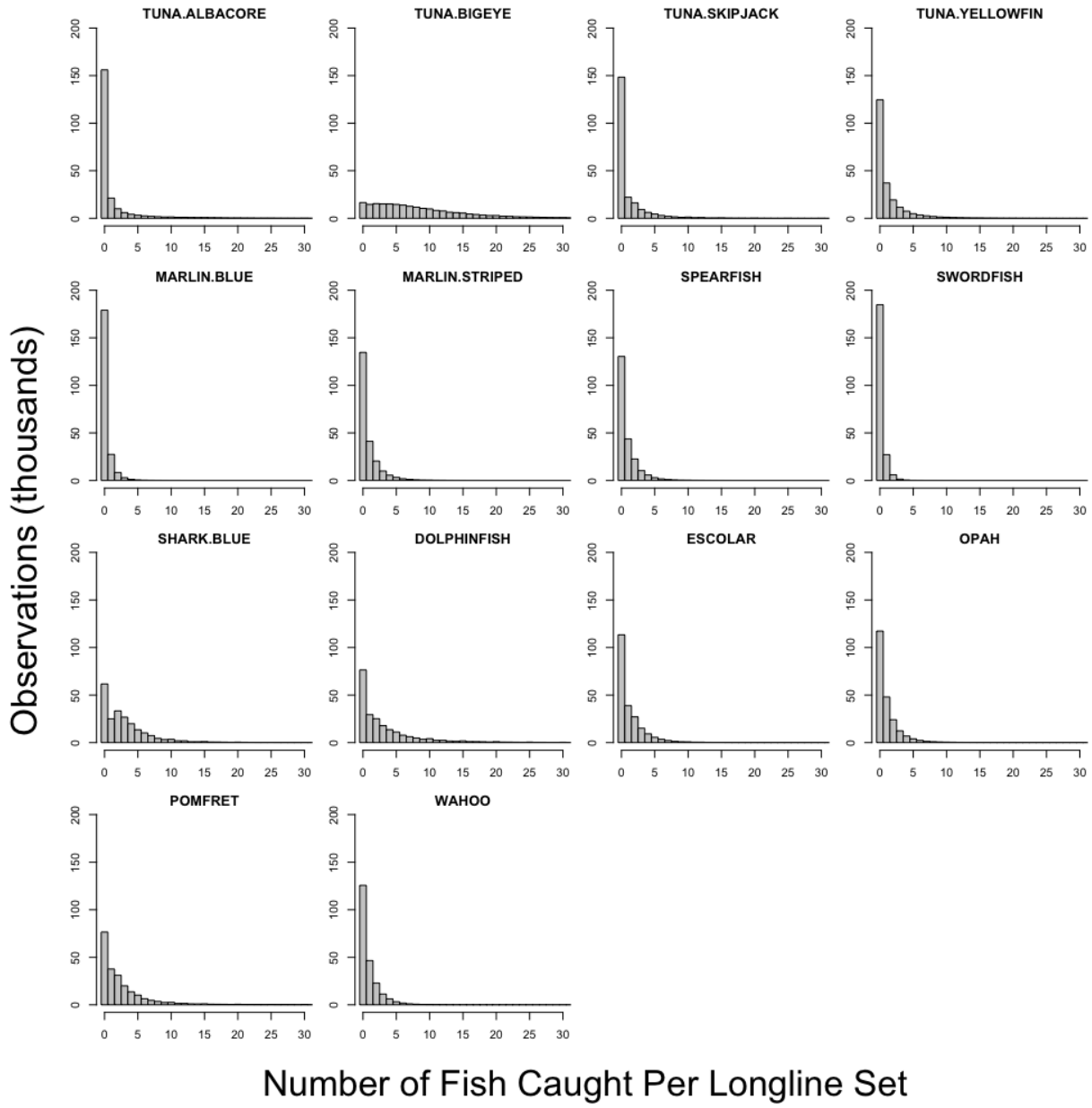

Figure S20: Catch data by species: Catch data distribution for each of the 14 pelagic predator species in the eddy-centric analysis. The x-axes were truncated at 30 to aid visualization.

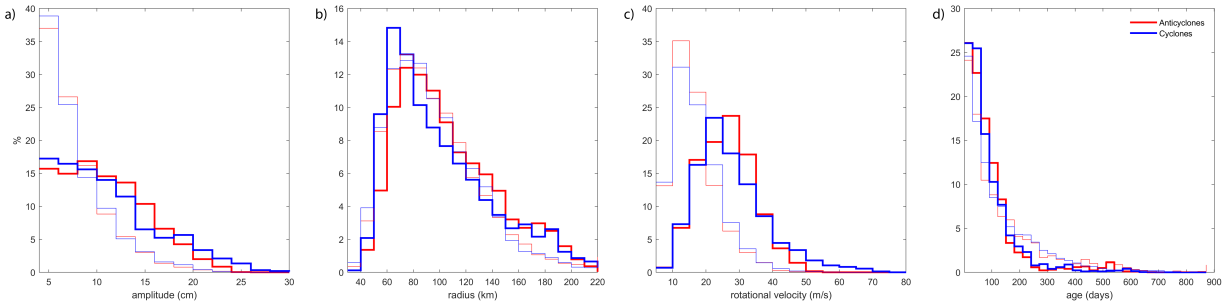

Figure S21: Eddy characteristics: Eddy characteristics of anticyclones (red) and cyclones (blue) in the high (bold colors) and low (faded colors) EKE subregions of the North Pacific Subtropical Gyre. Sample size (number of daily eddy realizations) – low EKE: anticyclones, n = 330,370; cyclones, n = 354,030 | high EKE: anticyclones, n = 217,090; cyclones, n = 226,320. Summary metrics provided in Table S8.

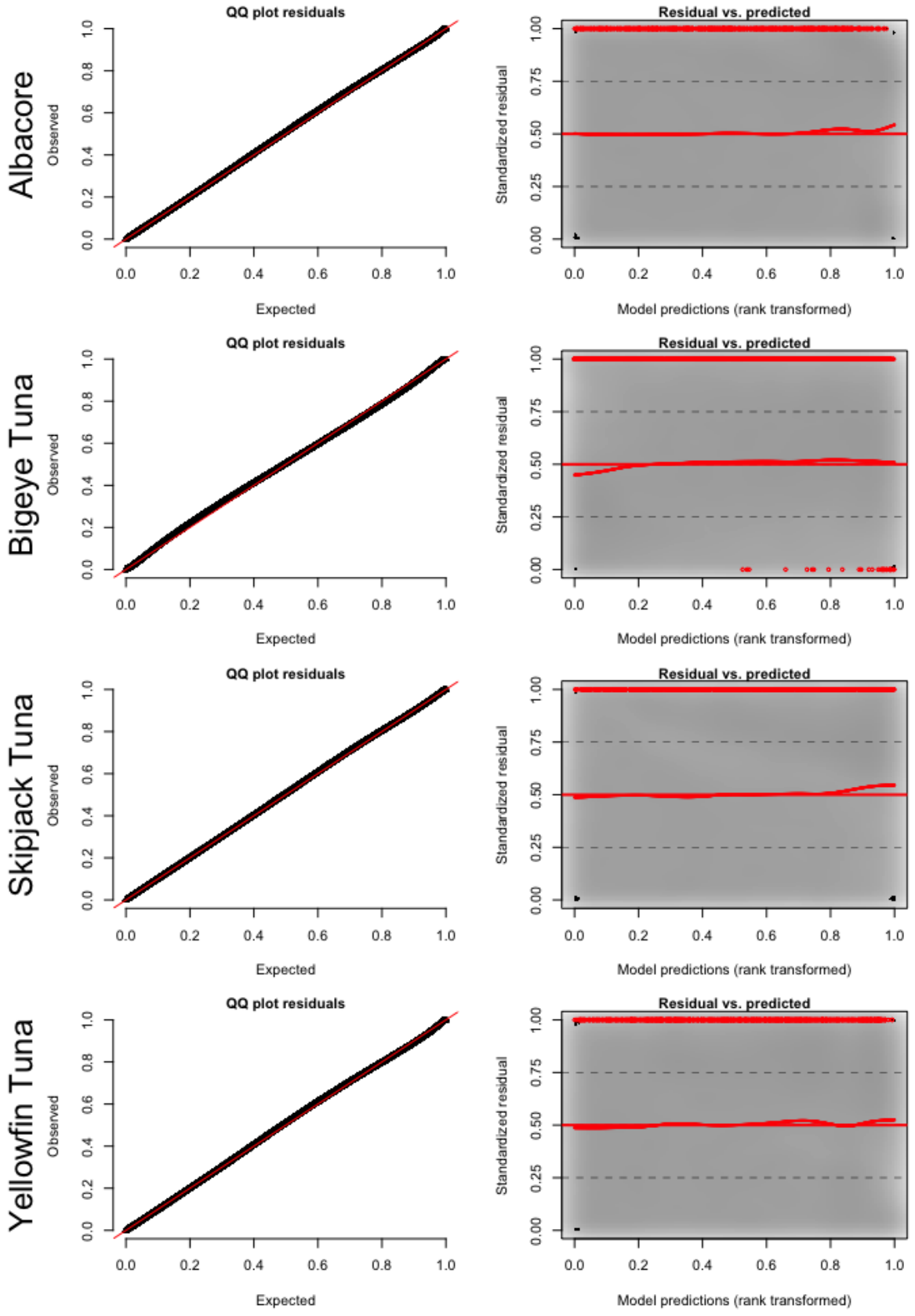

Figure S22: Eddy-Centric Analysis: Model diagnostics for tunas.

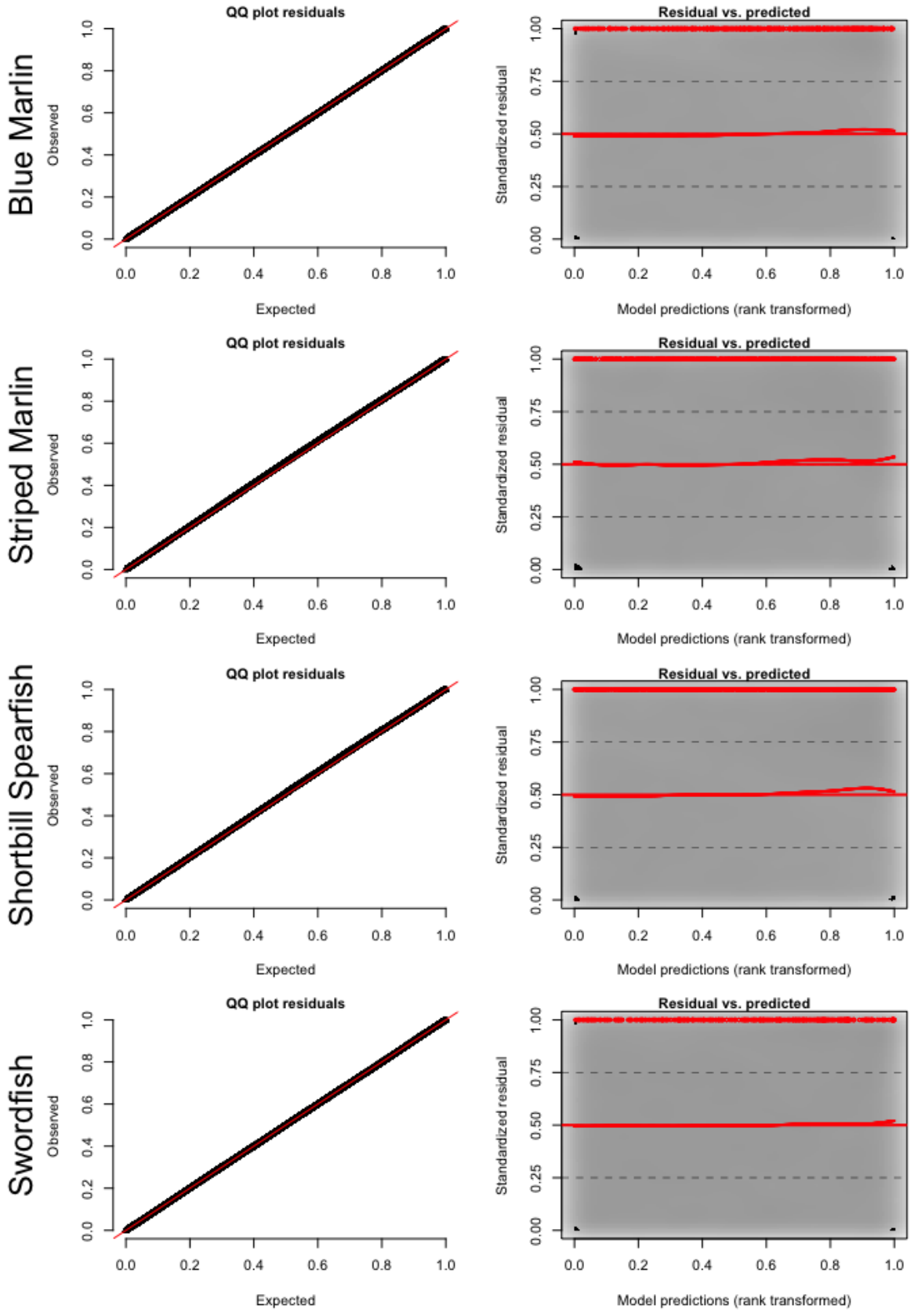

Figure S23: Eddy-Centric Analysis: Model diagnostics for billfishes.

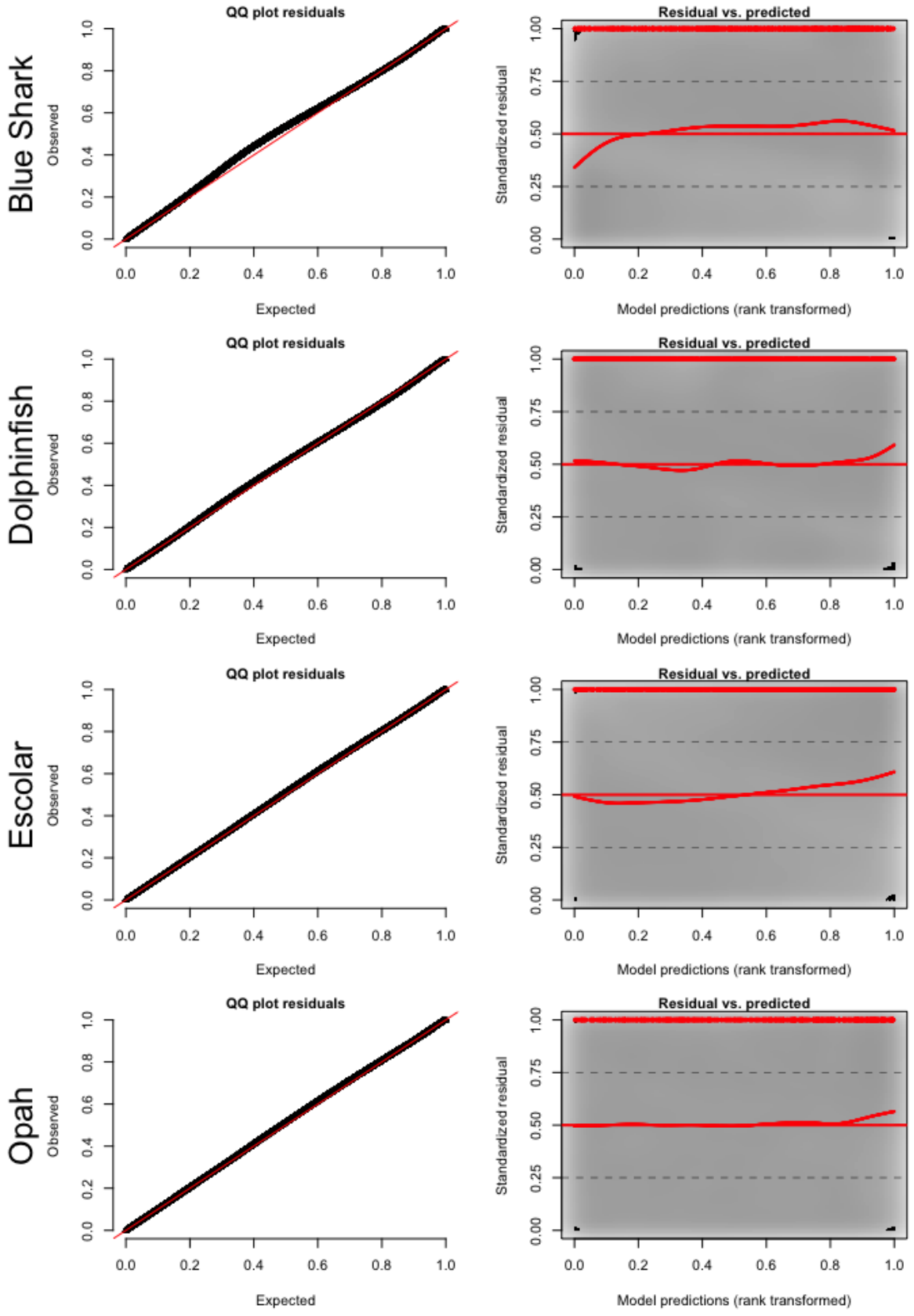

Figure S24: Eddy-Centric Analysis: Model diagnostics for sharks and other pelagic predators.

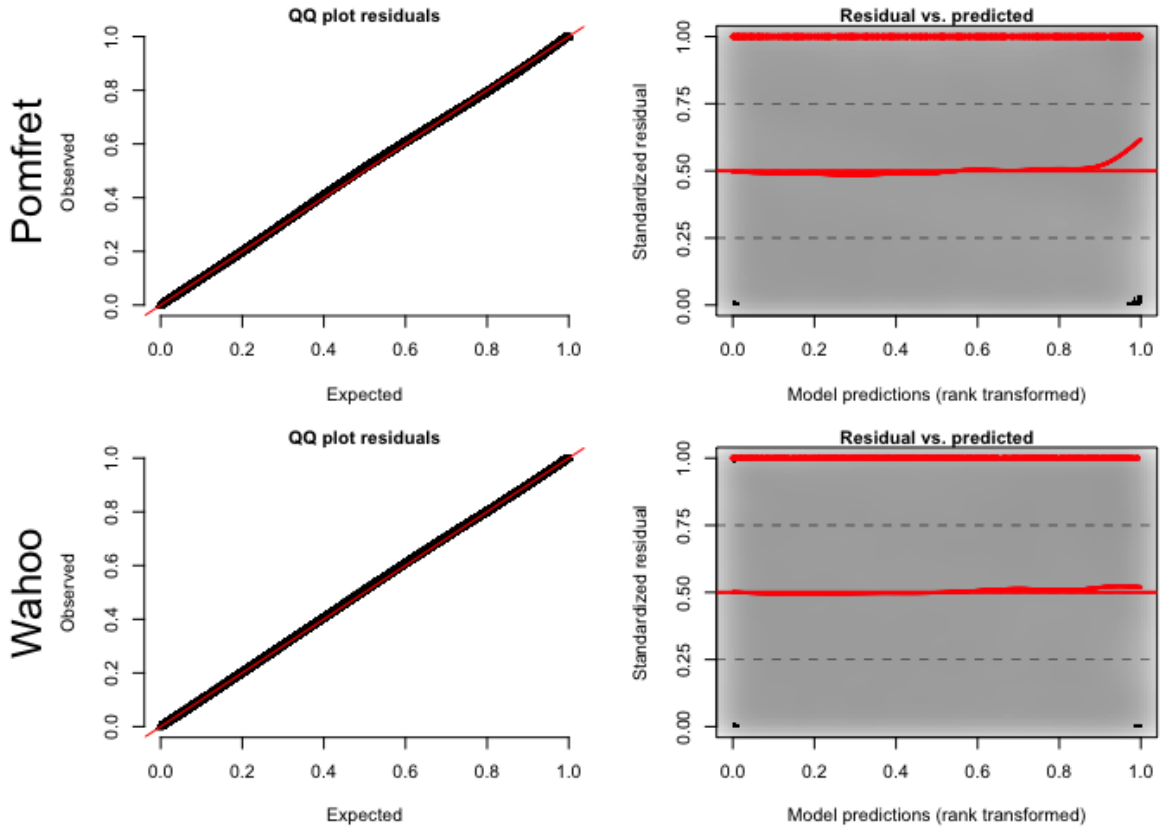

Figure S25: Eddy-Centric Analysis: Model diagnostics for other pelagic predators.

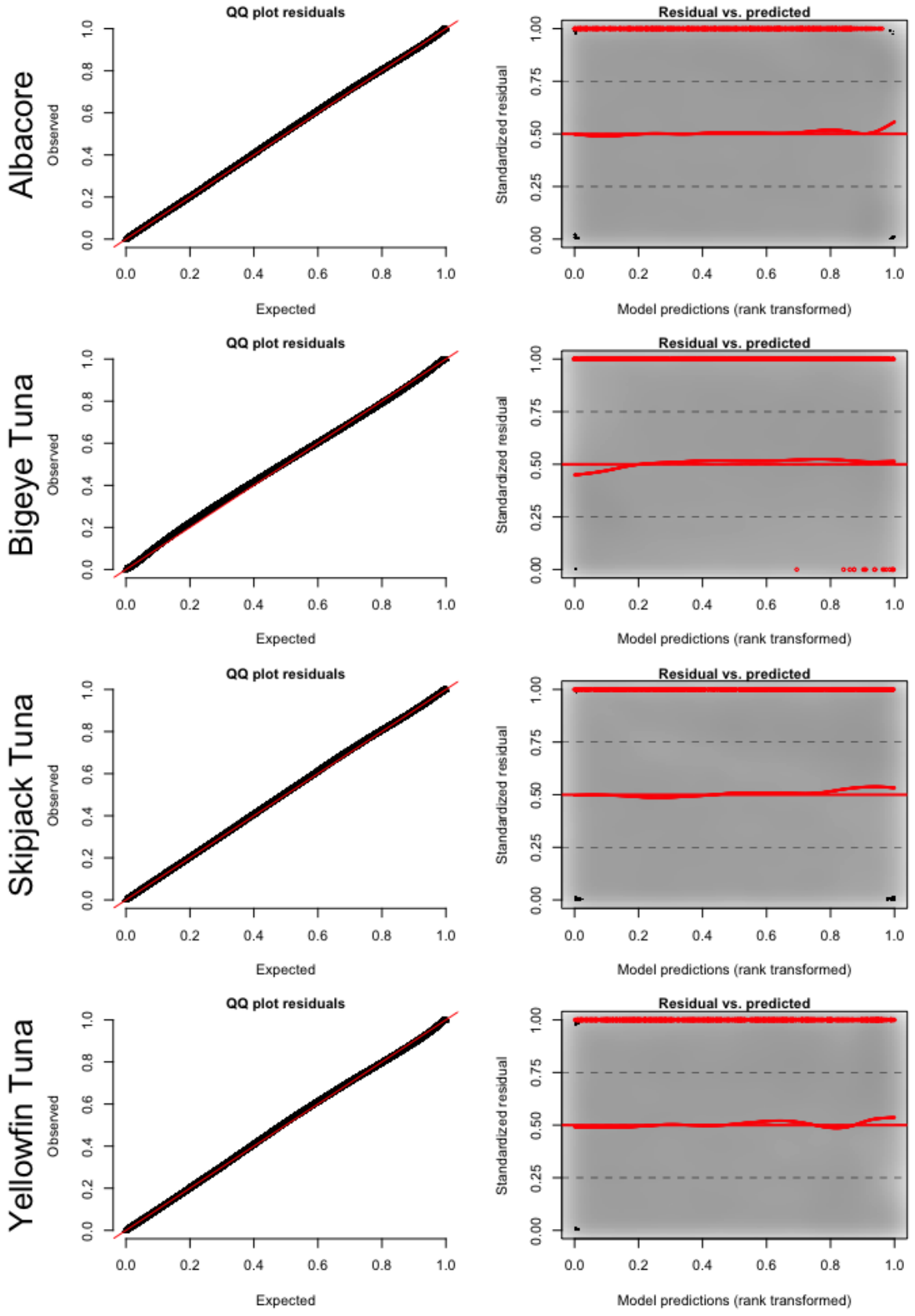

Figure S26: Complementary Analysis with Non-Eddy Baseline: Model diagnostics for tunas.

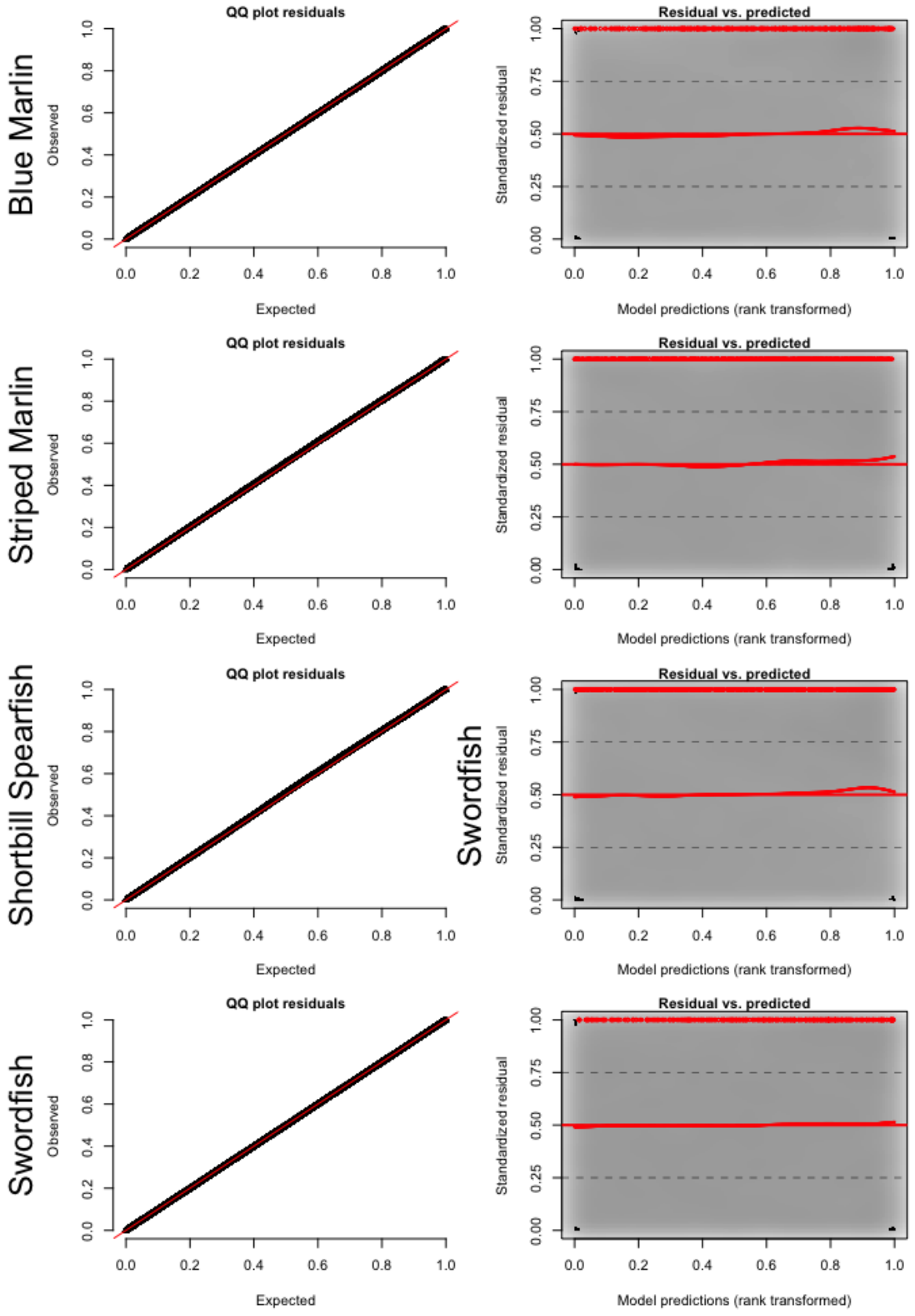

Figure S27: Complementary Analysis with Non-Eddy Baseline: Model diagnostics for billfishes.

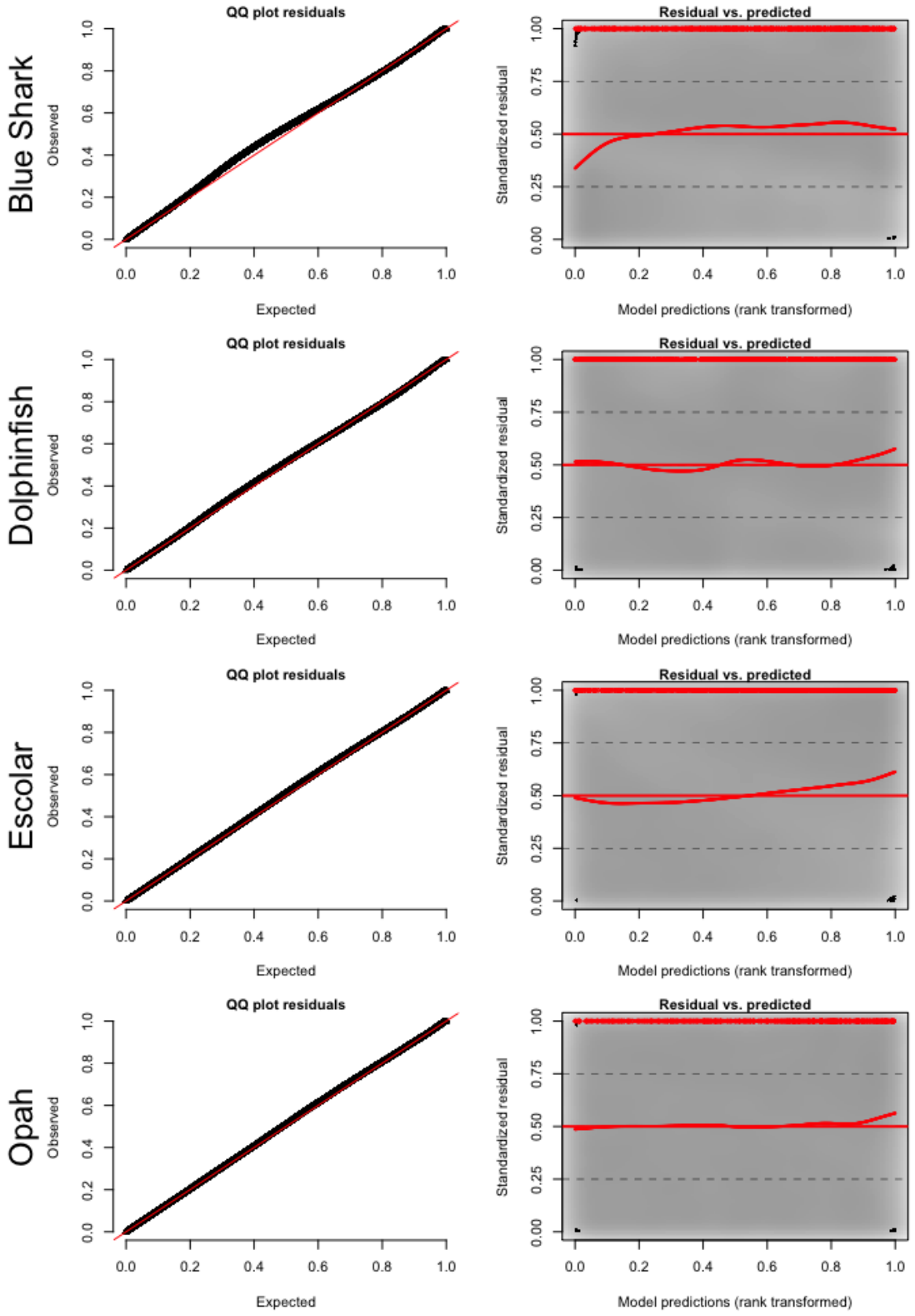

Figure S28: Complementary Analysis with Non-Eddy Baseline: Model diagnostics for sharks and other pelagic predators.

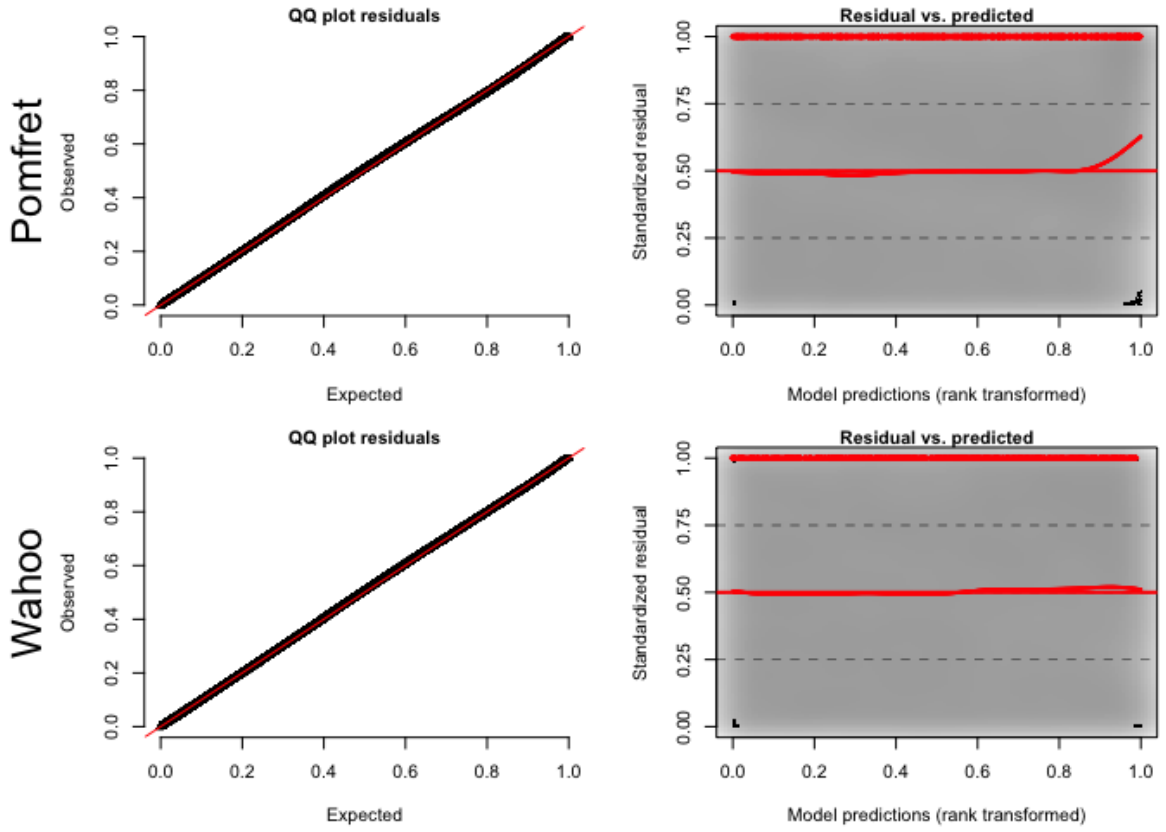

Figure S29: Complementary Analysis with Non-Eddy Baseline: Model diagnostics for other pelagic predators.

References

[1] Chaigneau, A., Gizolme, A. & Grados, C. Mesoscale eddies off Peru in altimeter records: Identification algorithms and eddy spatio-temporal patterns. *Progress in Oceanography* **79** (2-4), 106–119 (2008) .

[2] McGillicuddy Jr, D. J. *et al.* Influence of mesoscale eddies on new production in the Sargasso Sea. *Nature* **394**, 263–266 (1998) .

[3] Dufois, F. *et al.* Anticyclonic eddies are more productive than cyclonic eddies in subtropical gyres because of winter mixing. *Science Advances* **2** (5), 1–7 (2016). https://doi.org/10.1126/sciadv.1600282 .

[4] Godø, O. R. *et al.* Mesoscale eddies are oases for higher trophic marine life. *PLoS ONE* **7** (1), e30161 (2012). https://doi.org/10.1371/journal.pone.0030161 .

[5] Chelton, D. B., Gaube, P., Schlax, M. G., Early, J. J. & Samelson, R. M. The influence of nonlinear mesoscale eddies on near-surface oceanic chlorophyll. *Science* **334** (October), 328–333 (2011). https://doi.org/10.1126/science.1208897 .

[6] Sarmiento, J. L. *et al.* Response of ocean ecosystems to climate warming. *Global Biogeochemical Cycles* **18**, GB3003 (2004) .

[7] Bell, J. D. *et al.* Diversifying the use of tuna to improve food security and public health in Pacific Island countries and territories. *Marine Policy* **51**, 584–591 (2015) .

[8] Della Penna, A. & Gaube, P. Mesoscale eddies structure mesopelagic communities. *Frontiers in Marine Science* **7** (July), 454 (2020). https://doi.org/10.3389/fmars.2020.00454 .

[9] Braun, C. D. *et al.* The functional and ecological significance of deep diving by large marine predators. *Annual Review of Marine Science* **14**, 129–159 (2022) .

[10] McGillicuddy Jr, D. J. Mechanisms of physical-biological-biogeochemical interaction at the oceanic mesoscale. *Annual Review of Marine Science* **8**, 125–159 (2016) .

[11] Fennell, S. & Rose, G. Oceanographic influences on deep scattering layers across the North Atlantic. *Deep-Sea Research Part I: Oceanographic Research Papers* **105**, 132–141 (2015). URL http://dx.doi.org/10.1016/j.dsr.2015.09.002. https://doi.org/10.1016/j.dsr.2015.09.002 .

[12] Duffy, L. M. *et al.* Global trophic ecology of yellowfin, bigeye, and albacore tunas: understanding predation on micronekton communities at ocean-basin scales. *Deep-Sea Research Part II: Topical Studies in Oceanography* **140** (March), 55–73 (2017). https://doi.org/10.1016/j.dsr2.2017.03.003 .

[13] Gaube, P. *et al.* Mesoscale eddies influence the movements of mature female white sharks in the Gulf Stream and Sargasso Sea. *Scientific Reports* **8** (1), 1–8 (2018). https://doi.org/10.1038/s41598-018-25565-8 .

[14] Braun, C. D., Gaube, P., Sinclair-Taylor, T. H., Skomal, G. B. & Thorrold, S. R. Mesoscale eddies release pelagic sharks from thermal constraints to foraging in the ocean twilight zone. *Proceedings of the National Academy of Sciences of the United States of America* **116** (35), 17187–17192 (2019). https://doi.org/10.1073/pnas.1903067116 .

[15] Doyle, T. K. *et al.* Leatherback turtles satellite-tagged in European waters. *Endangered Species Research* **4**, 23–31 (2008) .

[16] Pauly, D. & Christensen, V. Primary production required to sustain global fisheries. *Letters to Nature* **374**, 255–257 (1995) .

[17] Lynham, J., Nikolaev, A., Raynor, J., Vilela, T. & Villaseñor-Derbez, J. C. Impact of two of the world's largest protected areas on longline fishery catch rates. *Nature Communications* **11** (1), 1–9 (2020). URL http://dx.doi.org/10.1038/s41467-020-14588-3. https://doi.org/10.1038/s41467-020-14588-3 .

[18] Polovina, J. J., Abecassis, M., Howell, E. A. & Woodworth, P. Increases in the relative abundance of mid-trophic level fishes concurrent with declines in apex predators in the subtropical North Pacific, 1996-2006. *Fishery Bulletin* **107**, 523–531 (2009) .

[19] Royer, T. C. Ocean eddies generated by seamounts in the North Pacific. *Science* **199** (4333), 1063–1064 (1978) .

[20] Liu, Y. *et al.* Eddy analysis in the subtropical zonal band of the North Pacific Ocean. *Deep-Sea Research Part I: Oceanographic Research Papers* **68**, 54–67 (2012). URL http://dx.doi.org/10.1016/j.dsr.2012.06.001. https://doi.org/10.1016/j.dsr.2012.06.001 .

[21] Bernstein, R. L. & White, W. B. Time and length scales of baroclinic eddies in the central North Pacific Ocean. *Journal of Physical Oceanography* **4** (4), 613–624 (1974). https://doi.org/10.1175/1520-0485(1974)004<0613:talsob>2.0.co;2 .

[22] Maunder, M. N. & Punt, A. E. Standardizing catch and effort data: a review of recent approaches. *Fisheries Research* **70**, 141–159 (2004). https://doi.org/10.1016/j.fishres.2004.08.002 .

[23] Woodworth, P. A. *et al.* Eddies as offshore foraging grounds for melon-headed whales (*Peponocephala electra*). *Marine Mammal Science* **28**, 638–647 (2012) .

[24] Gaube, P. *et al.* The use of mesoscale eddies by juvenile loggerhead sea turtles (*Caretta caretta*) in the southwestern Atlantic. *PLoS ONE* **12** (3) (2017). https://doi.org/10.1371/journal.pone.0172839 .

[25] Chambault, P. *et al.* Swirling in the ocean: immature loggerhead turtles seasonally target old anticyclonic eddies at the fringe of the North Atlantic Gyre. *Progress in Oceanography* **175** (May), 345–358 (2019). URL https://doi.org/10.1016/j.pocean.2019.05.005. https://doi.org/10.1016/j.pocean.2019.05.005 .

[26] Gaube, P., McGillicuddy Jr, D., Chelton, D., Behrenfeld, M. & Strutton, P. Regional variations in the influence of mesoscale eddies on near-surface chlorophyll. *Journal of Geophysical Research - Oceans* **119** (2014) .

[27] Waga, H., Kirawake, T. & Ueno, H. Impacts of mesoscale eddies on phytoplankton size structure. *Geophysical Research Letters* **46**, 13191–13198 (2019) .

[28] Irigoien, X. *et al.* Large mesopelagic fishes biomass and trophic efficiency in the open ocean. *Nature Communications* **5**, 3271 (2014) .

[29] Chen, Y.-l. L. *et al.* Biologically active warm-core anticyclonic eddies in the marginal seas of the western Pacific Ocean. *Deep Sea Research Part I: Oceanographic Research Papers* **106**, 68–84 (2015) .

[30] Harke, M. J. *et al.* Microbial community transcriptional patterns vary in response to mesoscale forcing in the North Pacific Subtropical Gyre. *Environmental Microbiology* **23**, 4807–4822 (2021) .

[31] Hawco, N. J. *et al.* Iron depletion in the deep chlorophyll maximum: mesoscale eddies as natural iron fertilization experiments . *Global Biogeochemical Cycles* **35**, e2021GB007112 (2021) .

[32] Klevjer, T. A. *et al.* Large scale patterns in vertical distribution and behaviour of mesopelagic scattering layers. *Scientific Reports* **6**, 1–11 (2016). https://doi.org/10.1038/srep19873 .

[33] Behrenfeld, M. J. *et al.* Global satellite-observed daily vertical migrations of ocean animals. *Nature* **576** (7786), 257–261 (2019). URL http://dx.doi.org/10.1038/s41586-019-1796-9. https://doi.org/10.1038/s41586-019-1796-9 .

[34] Madigan, D. J. *et al.* Water column structure defines vertical habitat of twelve pelagic predators in the South Atlantic. *ICES Journal of Marine Science* **78**, 867–883 (2021). https://doi.org/10.1093/icesjms/fsaa222 .

[35] Arostegui, M., Gaube, P. & Braun, C. Movement ecology and stenothermy of satellite-tagged shortbill spearfish (*Tetrapturus angustirostris*). *Fisheries Research* **215**, 21–26 (2019) .

[36] Lehodey, P., Senina, I. & Murtugudde, R. A spatial ecosystem and populations dynamics model (SEAPODYM) – modeling of tuna and tuna-like populations. *Progress in Oceanography* **78**, 304–318 (2008) .

[37] Varghese, S. P., Somvanshi, V. S. & Dalvi, R. S. Diet composition, feeding niche partitioning and trophic organisation of large pelagic predatory fishes in the eastern Arabian Sea. *Hydrobiologia* **736**, 99–114 (2014). https://doi.org/10.1007/s10750-014-1895-4 .

[38] Ward, P. & Myers, R. A. Inferring the depth distribution of catchability for pelagic fishes and correcting for variations in the depth of longline fishing gear. *Canadian Journal of Fisheries and Aquatic Sciences* **62** (5), 1130–1142 (2005). URL http://www.nrcresearchpress.com/doi/abs/10.1139/f05-021. https://doi.org/10.1139/f05-021 .

[39] Kai, E. T. *et al.* Top marine predators track Lagrangian coherent structures. *Proceedings of the National Academy of Sciences of the United States of America* **106** (20), 8245–8250 (2009). https://doi.org/10.1073/pnas.0811034106 .

[40] Lima, I. D., Olson, D. B. & Doney, S. C. Biological response to frontal dynamics and mesoscale variability in oligotrophic environments: biological production and community structure. *Journal of Geophysical Research: Oceans* **107** (8), 1–21 (2002). https://doi.org/10.1029/2000jc000393 .

[41] Spall, S. A. & Richards, K. J. A numerical model of mesoscale frontal instabilities and plankton dynamics - I. model formulation and initial experiments. *Deep-Sea Research Part I: Oceanographic Research Papers* **47** (7), 1261–1301 (2000). https://doi.org/10.1016/S0967-0637(99)00081-3 .

[42] Siegelman, L., O'Toole, M., Flexas, M., Rivière, P. & Klein, P. Submesoscale ocean fronts act as biological hotspot for southern elephant seal. *Scientific Reports* **9** (1), 1–13 (2019). https://doi.org/10.1038/s41598-019-42117-w .

[43] Lévy, M., Ferrari, R., Franks, P. J., Martin, A. P. & Rivière, P. Bringing physics to life at the submesoscale. *Geophysical Research Letters* **39** (14), 1–13 (2012). https://doi.org/10.1029/2012GL052756 .

[44] Guidi, L. *et al.* Does eddy-eddy interaction control surface phytoplankton distribution and carbon export in the North Pacific Subtropical Gyre? *Journal of Geophysical Research: Biogeosciences* **117** (2), 1–12 (2012). https://doi.org/10.1029/2012JG001984 .

[45] Chow, C. H., Cheah, W., Tai, J. H. & Liu, S. F. Anomalous wind triggered the largest phytoplankton bloom in the oligotrophic North Pacific Subtropical Gyre. *Scientific Reports* **9** (1), 1–11 (2019). URL http://dx.doi.org/10.1038/s41598-019-51989-x. https://doi.org/10.1038/s41598-019-51989-x .

[46] Guo, M., Xiu, P., Chai, F. & Xue, H. Mesoscale and submesoscale contributions to high sea surface chlorophyll in subtropical gyres. *Geophysical Research Letters* **46**, 13217–13226 (2019) .

[47] Klein, P. *et al.* Ocean-scale interactions from space. *Earth and Space Science* **6** (5), 795–817 (2019). https://doi.org/10.1029/2018EA000492 .

[48] Martin, A. *et al.* The oceans' twilight zone must be studied now, before it is too late. *Nature* **580**, 26–28 (2020) .

[49] St. John, M. A. *et al.* A dark hole in our understanding of marine ecosystems and their services: perspectives from the mesopelagic community. *Frontiers in Marine Science* **3**, 31 (2016) .

[50] Bigelow, K., Musyl, M. K., Poisson, F. & Kleiber, P. Pelagic longline gear depth and shoaling. *Fisheries Research* **77** (2), 173–183 (2006). https://doi.org/10.1016/j.fishres.2005.10.010 .

[51] Brodziak, J. & Walsh, W. A. Model selection and multimodel inference for standardizing catch rates of bycatch species: a case study of oceanic whitetip shark in the Hawaii-based longline fishery. *Canadian Journal of Fisheries and Aquatic Sciences* **70** (12), 1723–1740 (2013). https://doi.org/10.1139/cjfas-2013-0111 .

[52] Woodworth-Jefcoats, P. A., Polovina, J. & Drazen, J. Synergy among oceanographic variability, fishery expansion, and longline catch composition in the central North Pacific Ocean. *Fishery Bulletin* **116**, 228–239 (2018). https://doi.org/10.7755/FB.116.3-4.2.The .

[53] Boggs, C. H. Depth, capture time, and hooked longevity of longline-caught pelagic fish: timing bites of fish with chips. *Fishery Bulletin* **90** (4), 642–658 (1992) .

[54] Walsh, W. A. & Brodziak, J. Applications of Hawaii longline fishery observer and logbook data for stock assessment and fishery research. *NOAA Technical Memorandum* **NOAA-TM-NMFS-PIFSC-57**, 62 p. + Appendices (2016) .

[55] Walsh, W. A. & Brodziak, J. Billfish CPUE standardization in the Hawaii longline fishery: model selection and multimodel inference. *Fisheries Research* **166**, 151–162 (2015) .

[56] Gilman, E., Chaloupka, M., Fitchett, M., Cantrell, D. L. & Merrifield, M. Ecological responses to blue water MPAs. *PLoS ONE* **15**, e0235129 (2020) .

[57] Portner, E. J., Polovina, J. J. & Choy, C. A. Patterns in micronekton diversity across the North Pacific Subtropical Gyre observed from the diet of longnose lancetfish (*Alepisaurus ferox*). *Deep-Sea Research Part I* **125**, 40–51 (2017) .

[58] Brooks, M. E. *et al.* glmmTMB balances speed and flexibility among packages for zero-inflated generalized linear mixed modeling. *The R Journal* **9** (2), 378–400 (2017). URL https://journal.r-project.org/archive/2017/RJ-2017-066/index.html .

[59] Hartig, F. *DHARMa: residual diagnostics for hierarchical (multi-level / mixed) regression models* (2020). URL http://florianhartig.github.io/DHARMa/. R package version 0.3.3.0.

[60] Jackson, C. H. Multi-state models for panel data: the msm package for R. *Journal of Statistical Software* **38** (8), 1–29 (2011). URL http://www.jstatsoft.org/v38/i08/ .

[61] Bates, D. *et al. lme4: linear mixed-effects models using 'Eigen' and S4* (2020). URL https://github.com/lme4/lme4/. R package version 1.1-25.

[62] Lenth, R. *et al. emmeans: estimated marginal means, aka least-squares mean* (2022). URL https://github.com/rvlenth/emmeans. R package version 1.7.2.

[63] R Core Team. R: a language and environment for statistical computing (2020). URL http://www.r-project.org/.